

Two-dimensional carbon leading to new photoconversion processes

Q1 Q2
Q3 10

Cite this: DOI: 10.1039/c3cs60437c

Hongjie Tang,^{ab} Colin M. Hessel,^a Jianguan Wang,^{ab} Nailiang Yang,^{ab} Ranbo Yu,^{*c} Huijun Zhao^d and Dan Wang^{*a}

Two-dimensional (2D) carbon allotropes, which are atomic thick layers made of network carbon atoms with hexagonal structured lattices, have been neglected until the direct investigation of mechanically exfoliated graphene by Novoselov *et al.* in 2004. Graphene is a 2D carbon allotrope with a unique structure of hexagonally arranged atoms that give it unparalleled electrical conductivity and carrier mobility, in addition to excellent mechanical flexibility and extremely high specific surface area. Graphene and its derivatives have been extensively studied for photovoltaic and photocatalytic applications due to their inherent nature to extract and transport charges from photon-absorbing semiconductors and conjugated polymers. Graphyne and graphdiyne, 2D carbon allotropes like graphene but containing not only doubly but also triply bonded carbon atoms, are predicted to possess intrinsic semiconductor bandgap and even more superior electrical properties than graphene. The current theoretical understanding and experimental status of graphyne and graphdiyne will be discussed in contrast of graphene, demonstrating those promising competitors to graphene in further lightening a new photoconversion. This review addresses the recent successes and current challenges of graphene, graphyne and graphdiyne, and provides insightful perspectives for the future applications of 2D carbon materials in photoelectric conversion and photocatalysis.

Received 30th November 2013

DOI: 10.1039/c3cs60437c

www.rsc.org/csr

Key learning points

- (1) Comprehensive overview of recent advances in synthesis and chemical functionalization of graphene.
- (2) Design and function of graphene incorporated into dye-sensitized solar cells and organic photovoltaics.
- (3) Summary of photocatalytic application of graphene-based composites in organic transformations and water splitting.
- (4) Recent theoretical and experimental advances in graphyne and graphdiyne.
- (5) Summary and perspectives of 2D carbon allotropes in photoconversion applications.

1. Introduction

Over the past two decades there have been tremendous efforts to harness and utilize sunlight to drive chemical reactions and provide a renewable and sustainable source of power for the planet. In an effort to achieve such (much needed) goals there

have been numerous studies aiming to fabricate efficient photoconversion devices such as photovoltaics and photocatalytic reactors, which are designed around photoabsorbing semiconductors or conjugated polymeric materials that absorb solar energy to form electron-hole pairs (excitons) that are extracted to perform its best. The solar spectrum is composed of predominantly low energy electromagnetic radiation, with 95% of the photon energies lying below 3.2 eV (388 nm), making light harvesting and device efficiency of the utmost importance. Photoconversion efficiency is dependent on three main factors: (1) charge generation—the formation of excitons, (2) charge separation—the separation of electrons from holes, and (3) charge extraction/transport—the removal of electrons and holes from the photoabsorber to an external circuit or active surface. While charge generation relies on the optical and electronic properties of the photoabsorber, the device

^a State Key Laboratory of Multi-phase Complex Systems, Institute of Process Engineering, Chinese Academy of Sciences, Beijing 100190, P. R. China. E-mail: danwang@mail.ipe.ac.cn

^b University of Chinese Academy of Sciences, No. 19A Yuquan Road, Beijing 100049, P. R. China

^c Department of Physical Chemistry, School of Metallurgical and Ecological Engineering, University of Science and Technology Beijing, Beijing 100083, P. R. China. E-mail: ranboyu@ustb.edu.cn

^d Centre for Clean Environment and Energy, Gold Coast Campus, Griffith University, Queensland 4222, Australia

1 architecture, layer composition, and additives largely affect the
charge separation and extraction efficiency. To date, graphene
has been demonstrated to be the single most important material
capable of enhancing the efficiency of photoconversion
5 devices, which will lead to new photoconversion processes.

Graphene is a single layer of sp^2 -bonded carbon atoms
arranged in a honeycomb lattice and is the latest carbon
allotrope to gain international acclaim. Its unique set of optical,
electronic, and mechanical properties has made it arguably the
10 most effective additive for enhancing photoconversion efficiency
in photovoltaic and photocatalytic devices.¹ Single
layered graphene is a zero-gap semimetal that exhibits ballistic

charge transport (electrical conductivity $\sim 10^8$ S m^{-1}) and
exceptionally high carrier mobility (20 000 cm^2 V^{-1} s^{-1}), making
it an excellent candidate for improving charge extraction
and transport. Graphene sheets are also flexible, with a large
theoretical specific surface area of 2630 m^2 g^{-1} , allowing them
5 to readily interpenetrate with semiconductor nanoparticles and
conjugated polymers to create electronic bridges. Notably for
photo-related applications, graphene also has exceptional optical
transmittance ($\sim 97.7\%$ at 550 nm), and is currently a top
candidate for replacing indium tin oxide (ITO) as a high
10 performance and cost-effective transparent conductive electrode
material.



Hongjie Tang

Hongjie Tang received his BE from the Department of Materials Science and Engineering at China University of Geosciences, Beijing. He is currently a PhD candidate under the supervision of Prof. Dan Wang from State Key Laboratory of Multi-phase Complex Systems at the Institute of Process Engineering, Chinese Academy of Sciences. His current research interests are focused on the design and synthesis of

nanomaterials for energy and environmental applications.



Colin M. Hessel

Colin M. Hessel received his BSc and PhD in materials chemistry at the University of Alberta (2004 and 2008) under the supervision of Dr Jonathan Veinot. He worked with Dr Brian A. Korgel as an NSERC postdoctoral fellow in the Department of Chemical Engineering at the University of Texas at Austin until 2012. He is currently a Young International Research Fellow at The Institute of Process Engineering, Chinese Academy of Sciences in Beijing.

His research interests include inorganic materials synthesis, surface chemistry, and photocatalysis, with focus on the development and application of nanomaterials that interact favourably with electromagnetic radiation, particularly semiconductor nanocrystals, plasmonic metals, and photovoltaic materials.



Jiangyan Wang

Jiangyan Wang received her BE from the School of Chemical and Environmental Engineering in 2010 at the China University of Mining and Technology, Beijing. She is currently studying for her PhD degree under the supervision of Prof. Dan Wang from State Key Laboratory of Multi-phase Complex Systems at the Institute of Process Engineering, Chinese Academy of Sciences. Her current research interests are focused on the design and

synthesis of micro-/nano-structured functional inorganic materials nanomaterials for energy conversion and storage, such as lithium ion battery, supercapacitors.



Dan Wang

Dan Wang received his BS and MS at Jilin University (1994 and 1997) and PhD at Yamanashi University (2001). In 2004, he was awarded the Hundred Talents Program of the Chinese Academy of Sciences and took his current position as a Principal Investigator at the State Key Laboratory of Multi-phase Complex Systems, Institute of Process Engineering, Chinese Academy of Sciences. His research interests include

inorganic material chemistry, surface and colloidal chemistry, hydrothermal chemistry, sol-gel chemistry and self-assembly processes, with focus on the design and synthesis of micro-/nano-structured functional inorganic materials and their applications in energy conversion and storage, photocatalysis and sensors.

1 Since the seminal reports on graphene, there has been a
 2 flurry of research focused on increasing production yield and
 3 designing chemical functionalization schemes to facilitate
 4 incorporation of graphene in charge transport limited devices,
 5 particularly photoconversion devices. As it stands, however, not
 6 all graphenes are created equally, and there currently exists a
 7 dichotomy between structure and function.² Methods that
 8 produce high fidelity graphene with excellent electronic prop-
 9 erties, such as chemical vapor deposition, epitaxial growth on
 10 silicon carbide, and manual mechanical cleavage of graphite,
 11 produce low yields of hydrophobic, chemically inert graphene,
 12 limiting their application in commercial devices. On the other
 13 hand, the solution-based oxidation–exfoliation–reduction of
 14 graphite to graphene produces large quantities of hydrophilic,
 15 chemically versatile graphene sheets. This type of graphene is
 16 readily formed into composites, dispersed in solvents, and is
 17 amenable to large-scale production. Unfortunately, it also con-
 18 tains numerous defects that degrade electrical performance. As
 19 a result, researchers aiming to improve the performance of
 20 photoconversion devices are forced to compromise between
 21 structure and function when designing their devices.

22 To date, graphene-based materials have been successfully
 23 incorporated into a variety of photoconversion devices and
 24 consistently demonstrate marked improved efficiency. Signifi-
 25 cant progress has been made in the chemical modification of
 26 graphene with small organic molecules or polymers, inorganic
 27 nanocrystals and dopant atoms (*e.g.*, nitrogen, boron).³
 28 Solution-processable graphene has been incorporated into
 29 functional films and composites for transparent electrodes,
 30 solar cells, and photocatalysts.⁴ Under such circumstances,
 31 graphene enhances charge extraction and transport by improv-
 32 ing interfacial contact and charge carrier mobility in the
 33 devices. By designing solution-based methods to yield high-
 34 quality graphene, it is expected that the device efficiencies
 35 would be dramatically improved and the utilization of gra-
 36 phene would become the ubiquitous strategy.

37 Graphyne and graphdiyne, two new and hotly debated 2D
 38 carbon allotropes, contain two diacetylenic linkages between a
 39 repeating pattern of carbon hexagons. Like graphene, they are
 40 also a one-atom-thick sheet of carbon atoms but with both *sp*
 41 and *sp*² hybridized carbon bonds. The presence of the *sp*
 42 carbon atoms disintegrates the original honeycomb lattice of
 43 graphene. As a result, multiple lattice types of graphyne with
 44 different geometry arise. Despite the similarity between gra-
 45 phene and graphyne in topology, graphynes exhibit rich physi-
 46 cal properties that are quite different from those of graphene
 47 due to the presence of the acetylenic linkages.⁵ For example,
 48 graphdiyne has a very large in-plane Young's modulus of <412
 49 GPa, a value as large as that of the silicon carbide (<450 GPa)
 50 and <40% of that in graphene and diamond (<1100 GPa).
 51 However, unlike graphene, graphyne and graphdiyne display
 52 inherent semiconducting characteristics and their transport
 53 properties are associated with the length of C link in their
 54 structures. Previous first-principles electronic structure calcu-
 55 lations have shown that graphynes exhibit small carrier effective
 56 masses and high carrier mobility like graphene, and α -, β -, and

57 6,6,12-graphynes also possess Dirac cone-like band structures
 58 at the Fermi level, regardless of the existence or absence of the
 59 hexagonal (*p6m*) symmetry. Especially 6,6,12-graphyne, which
 60 have exceptional directional-dependent electronic properties, is
 61 predicted to have intrinsic mobility of $4.29 \times 10^5 \text{ cm}^2 \text{ V}^{-1} \text{ s}^{-1}$
 62 for holes and $5.41 \times 10^5 \text{ cm}^2 \text{ V}^{-1} \text{ s}^{-1}$ for electrons at room
 63 temperature, larger than that of graphene ($<3 \times 10^5 \text{ cm}^2 \text{ V}^{-1}$
 64 s^{-1}). Only recently, large area graphdiyne films have been
 65 successfully synthesized on the surface of copper *via* a cross-
 66 coupling reaction. It exhibits excellent semiconducting prop-
 67 erties and the conductivity of graphdiyne films reaches $10^{-3} \sim$
 68 10^{-4} S m^{-1} at room temperature. When used in photovoltaic
 69 and photocatalytic devices, it can form large interfaces with
 70 photon-adsorbing semiconductors and organic molecules, per-
 71 forming as well as, if not much better than graphene, implying
 72 it is a very promising competitor to graphene in photoconver-
 73 sion. Also the intrinsic semiconductor bandgap, combined with
 74 the superior carrier mobility, give us full confidence that in the
 75 future, together with graphene, graphyne and graphdiyne will
 76 further provide new photoconversions.

77 In this tutorial review, we provide a comparative summary of
 78 current state-of-the-art methods to produce and functionalize
 79 graphene, and systematically discuss recent outstanding
 80 achievements in graphene-based materials in photoelectric
 81 conversion and photocatalysis, such as transparent electrodes,
 82 solar cells, photo-degradation, water splitting and organic
 83 transformations (Fig. 1). The current status and challenges
 84 associated with transparent electrodes, dye-sensitized solar
 85 cells, organic photovoltaics and photocatalytic applications
 86 are explained to reveal the critical role of graphene played in
 87 revolutionizing the design, fabrication and performance
 88 enhancement of photoconversion devices. Graphyne and
 89 graphdiyne, two other 2D carbon allotropes, are also intro-
 90 duced as next-generation materials in the carbon family. The
 91 theoretical prediction and experimental advances in graphyne
 92 and graphdiyne will be discussed and compared with graphene,
 93 revealing their great potential in photocatalysis and optoelec-
 94 tric conversion. Finally, we summarize and propose the

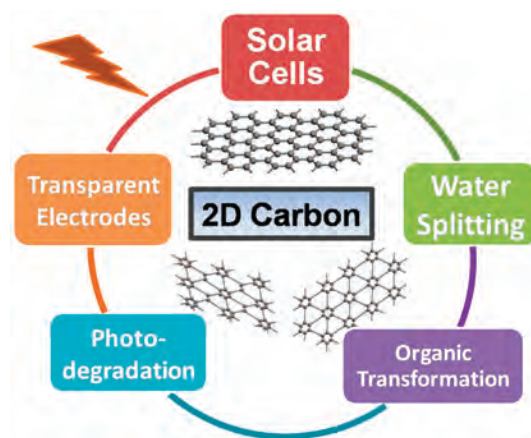


Fig. 1 Schematic illustration of the critical functions of 2D carbon in photoconversion.

1 confirmed benefits and future obstacles/challenges that 2D
2 carbon allotropes based nanocomposites may face in photo-
3 conversion applications.

5 2. Synthesis and functionalization of 6 graphene

7 2.1 Synthesis of graphene

10 Since graphene was initially isolated by mechanical exfoliation
11 of graphite ("Scotch tape" method),⁶ substantial progress has
12 been achieved in producing large area defect-free graphene *via*
13 chemical vapor deposition (CVD), vacuum annealing of silicon
14 carbide (SiC) and solution-based methods such as the oxidation-
15 exfoliation-reduction of graphite, each method has its
16 merits and drawbacks. In general, vapor-phase methods are
17 capable of producing high fidelity graphene but low-yield, while
18 solution-based approaches have an advantage of high-yield, but
19 products are defect-riddled materials. A key challenge is to
20 develop enabling synthetic methods capable of large-scale
21 production of high quality graphene with perfect 2D hexagonal
22 structure over long range and large areas that possess high
23 charge carrier mobility to ensure novel device performance.²

25 High-quality large area graphene sheets have been prepared
26 by CVD of gaseous carbon sources such as methane or acetylene
27 on copper or nickel substrates.⁷ Single-layered graphene
28 can be readily prepared *via* low pressure CVD of methane. An
29 increase in the molecular weight or partial pressure of the
30 carbon precursor results in the formation of bilayer or multi-
31 layer graphene sheets. The CVD produced graphene films are
32 easily removed from the growth substrates and transferred to a
33 variety of alternative substrates for preparation of high-quality
34 graphene-based transparent electrodes for solar cells and other
35 optoelectronic devices.

36 Also, ultra-high vacuum annealing of single crystal SiC with
37 treatment temperatures above 1100 °C is an effective means to
38 produce high-quality epitaxially grown graphene with tunable
39 electronic properties.⁸ Because the sublimation rate of silicon
40 is higher than carbon, the remaining carbon on the surface
41 rearranges to form graphene nanosheets, therefore, the dimen-
42 sions of formed graphene nanosheets are largely determined by
43 the size of SiC crystals. The graphene produced by this method
44 has been widely used to examine the fundamental electronic
45 properties of graphene such as electronic band structure and
46 charge carrier mobility. Nevertheless, this method is unsuitable
47 for massive production, making it a niche method that suits
48 fundamental studies.

49 Solution-based oxidation-exfoliation-reduction of graphite
50 to chemically converted graphene (CCG) is one of the most well-
51 developed and popular methods for quantity production of
52 single-layered graphene.⁹ Graphite is initially oxidized to gra-
53 phite oxide with KMnO_4 and NaNO_3 in concentrated H_2SO_4
54 (Fig. 2), followed by mechanical/chemical exfoliation to pro-
55 duce single layer graphene oxide (GO) sheets. Then GO is
56 converted to graphene with strong reductants such as hydrazine
57 (N_2H_4), which also restores the aromaticity of the single

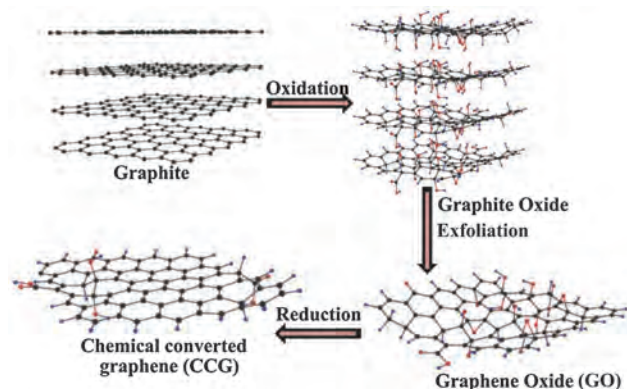


Fig. 2 Preparation of chemically converted graphene by oxidation of graphite. Reproduced with permission of Wiley from ref. 9. Copyright 2011.

layer carbon lattice. Compared with CVD grown graphene,
which has entered the single crystal era and shown comparable
quality and electronic properties to that of mechanical exfo-
liated graphene,⁷ the products obtained by this preparative
method often possess a considerable chemical, surface and
edge defects that disrupt the electronic network of graphene.
However, due to its low cost, high yield, simplicity and potential
for *in situ* chemical functionalization, it is the most effective
approach to obtain large quantity single layer graphene.

Graphene can also be obtained by non-oxidative wet-
chemical methods, such as direct exfoliation of graphite in
various solvents *via* sonication¹⁰ and intercalation.¹¹ Though
the resulting graphene materials have much fewer defects than
those of CCG, this method is not widely used because of its
elaborate procedures, unsatisfactory yield of single layer gra-
phene or sonication induced scissoring of graphene sheets into
very small sizes.

Nanosized graphene has also been shown to be synthesized
via organic coupling reactions.¹² This type of graphene with
a well-defined molecular structure can only be prepared through
bottom-up approaches and is usually called "nanographene"
due to the size of graphene sheets produced. The well-defined
structure of nanographene provides the ability to precisely
control the graphene bandgap, which is crucial for fundamen-
tal research and the future of graphene based solar cells.

2.2 Graphene functionalization

The surface and edge chemistry of graphene dramatically
affects its electronic properties, layer stacking modes, solution
processability, and the integration of graphene into existing
semiconductor fabrication processes. Pristine graphene sheets
are chemically inert and hydrophobic due to the lack of surface
functional groups. Chemical functionalization offers the oppor-
tunity to tailor the surface chemistry and transfer graphene into
the solution phase, which is a necessary step on the path to
commercialization.³ In addition to enhancing solubility, it can
also be used to tune the bandgap of graphene and induce
highly sought semiconducting properties. The creation of a
band gap through chemical functionalization is an attractive

1 method for producing semiconducting graphene for photocon-
version devices. For example, Haddon and co-workers
covalently attached aryl groups to the basal plane of graphene
by diazonium chemistry and observed the electronic transfor-
5 mation from near-metallic to semiconducting.¹³

Surface functionalization routes and solubilisation schemes
for graphene are predominantly derived from methods estab-
lished for graphite and carbon nanotubes (CNTs), but also
depend on the methods used to produce graphene. In general,
10 graphene is typically surface functionalized *via* (i) non-covalent
bonding, (ii) covalent C–C coupling reactions, and (iii) substi-
tutional doping.

2.2.1 Non-covalent functionalization. Non-covalent func-
tionalization of graphene is based on van der Waals forces or
15 π – π stacking of aromatic molecules on the graphene plane. It is
achieved by polymer wrapping, adsorption of surfactants or
small aromatic molecules, and interactions with porphyrins or
biomolecules such as DNA and peptides.³ In contrast to covalent
modification that introduces defects, it can improve the
20 solubility without disturbing the electronic network, which is
quite useful for application in photoconversion devices. For
example, CVD-grown graphene is hydrophobic and not solution
compatible with hydrophilic poly(3,4-ethylenedioxythiophene)
(PEDOT), the photoabsorber for organic photovoltaics (OPVs).
25 Non-covalent attaching pyrene derivatives such as PBASE (pyrene
butanoic acid succidimidyl ester) to the basal plane of
graphene improves the solution dispersibility of graphene and
enables its incorporation into OPV devices.

2.2.2 Covalent functionalization. Covalent functionaliza-
tion of pristine graphene and graphene oxide requires different
30 approaches. Pristine graphene can be functionalized with
organic molecules by the addition of free radicals to sp^2 carbon
atoms of graphene, or the addition of dienophiles to C–C
bonds. These routes impart chemical functionality that
improves the dispersibility of graphene in common organic
35 solvents, which is a necessary step enabling the formation of
composites with other functional materials. In addition, when
organic molecules are covalently attached to the graphene
surface, its extended aromatic character is perturbed, allowing
the control of electronic properties.
40

The oxidation of graphite to GO provides exfoliated carbon
nanosheets with a significant number of oxygen-containing
surface groups that enables its dispersibility in hydrophilic
solvents and subsequent chemical functionalization.⁹ The ideal
45 approach to covalent functionalization of graphene oxide is to
utilize orthogonal reactions to selectively functionalize one site
over another, such as at carboxylic acid group instead of at
epoxy group. In reality, however, the reactions are non-selective
and a range of chemistry occurs, thus obscuring the chemical
50 understanding purity of what is known as “graphene oxide”.
The incorporation of oxygen functional groups introduces
defects in the basal plane of graphene and disrupts the π -
conjugation, giving GO insulating properties and a defect
dominated optical gap. Therefore, if controllable, this method
55 offers the possibility to tune the electronic structure of GO by
the reduction or functionalization with specific electron donor/

acceptor molecules, highlighting the versatility of this route for
a wide range of applications.

2.2.3 Substitutional doping. Substitutional doping of gra-
phene with nitrogen or boron atoms induces n- or p-type
electronic behavior. Graphene chemical doping with electron-
5 withdrawing oxygen functionalities shows p-type properties,
while electron-donating nitrogen functionalities induce n-type
characteristics. Controlling the doping concentration provides
the ability to tailor the electronic properties of graphene,
thereby expanding its application in semiconductor-based
10 nanoelectronics. Electron-rich nitrogen dopants can be substi-
tuted for oxygen or carbon atoms during CVD growth of
graphene, annealing, arc discharge, or solvothermal methods.
Additionally, oxygen or sp^3 carbon atoms at defect sites in GO
can be substituted by nitrogen during high temperature
15 reduction with ammonia or hydrazine.¹⁴

3. Applications for photoelectric conversion

Graphene and its derivatives have been studied extensively for
photovoltaics due to its high optical transparency (absorbance
of only 2.3%), high thermal conductivity ($\sim 5000 \text{ W m}^{-1} \text{ K}^{-1}$),
high electrical conductivity (10^8 S m^{-1}), and excellent mechan-
25 ical flexibility. Graphene has typically been incorporated into
solar cells to enhance charge extraction and transport, but also
utilized as conductive transparent electrodes, and in dye-
sensitized solar cells (DSSCs) as the catalytic counter electrode
in place of standard platinum materials that are increasingly
30 rare and expensive.⁴

3.1 Transparent electrodes

Transparent electrodes (TEs) are a fundamental component for
thin-film and dye-sensitized solar cells as they allow light to
35 penetrate into the device and concomitantly extract photogen-
erated charges. Effective TEs should have low sheet resistance,
high transparency and appropriate work function depending
on the device architecture. Doped metal oxides, particularly
ITO, have been widely used as TE materials due to their low
40 sheet resistance (*e.g.*, 15–90 $\Omega \text{ sq}^{-1}$) and high optical transmittance
($>90\%$ at 550 nm). However, there has been a considerable
effort to find a more sustainable substitute for ITO due to:
(i) the limited abundance of indium in the earth's crust, (ii) its
poor stability in acidic or basic solutions, (iii) susceptibility to
45 ion diffusion into polymer layers, (iv) limited transparency in
the near-infrared region.

Graphene-based TEs can be fabricated *via* inexpensive
solution-based methods, and their work function can be engi-
50 neered *via* chemical doping, and covalent or non-covalent
functionalization. One of the most straightforward and con-
venient methods for producing large-area graphene TEs
involves the reduction of pre-fabricated graphene oxide thin
films. Eda *et al.* used vacuum filtration to obtain uniform films
55 of reduced graphene oxide (rGO) with a controllable number of
GO layers over large areas.¹⁵ Thermal and chemical reduction

1 were combined to repair the sp^2 structure and restore the
 conductivity. The lowest attainable sheet resistance was ~ 43
 $k\Omega\text{ sq}^{-1}$ at 550 nm, with transparency ranging from 60% to
 95%—still far from the requirements for practical applications
 5 (sheet resistance $< 100\ \Omega\text{ sq}^{-1}$, at $T > 90\%$).

The low conductivity of CCG thin films is attributed to
 structural defects resulting from remnant oxygen moieties
 and also the high contact resistance between graphene sheets.
 Thermal reduction is currently the most efficient approach to
 10 eliminate oxygen-containing moieties and can produce highly
 conductive CCG films of up to about $10^5\ \text{S m}^{-1}$, which is
 significantly higher than for chemical reduction *via* N_2H_4 alone
 ($5000\ \text{S m}^{-1}$). To reduce the sheet resistance of graphene films
 the sheets can be enlarged to reduce the total number of inter-
 layer contacts that impede conductivity. By adopting ultracentrifugation
 15 together with sonication in the CCG production
 protocol the process will preferentially yield larger graphene
 sheets. Kim *et al.* have also shown that bridging the CCG sheets
 with conducting nanomaterials is a simple and versatile
 20 method to produce graphene films with low sheet resistance
 of $8\ k\Omega\text{ sq}^{-1}$ with 81% transmittance at 550 nm.¹⁶ By integrat-
 ing MWCNTs (multi-walled carbon nanotubes) into thin films
 of rGO nanosheets *via* layer-by-layer (LBL) assembly, the hybrid
 films not only show enhanced electronic conductivity, but also
 25 afford mechanical flexibility by bridging the gaps between
 graphene sheets.

CVD is becoming one of the most promising routes to obtain
 high-quality, transferable and/or patterned graphene films with
 low sheet resistance. In contrast to solution-based production
 30 of graphene, CVD can easily yield large-area continuous gra-
 phene sheets with low inter-sheet resistance. For example, Bae
et al. reported the roll-to-roll production of 30-inch graphene
 films grown on flexible copper substrates by CVD.¹⁷ After wet
 chemical doping, the films have a sheet resistance as low as 125
 $\Omega\text{ sq}^{-1}$ with 97.4% optical transmittance. Using layer-by-layer
 35 deposition, a doped four-layer film with a sheet resistance of
 about $30\ \Omega\text{ sq}^{-1}$ and $< 90\%$ transparency was obtained, which
 is superior to commercial ITO transparent electrodes. Combin-
 ing the scalability of CVD graphene film production with the
 processability of roll-to-roll deposition, it is anticipated that the
 40 commercial production of large-scale transparent electrodes
 will soon be realized.

In practice, graphene TEs have been utilized for flexible thin
 film OPVs. Yin and co-workers utilized rGO transparent elec-
 45 trodes for flexible OPV devices with 0.78 photoconversion
 efficiency.¹⁸ RGO was transferred onto polyethylene terephthal-
 ate (PET) substrates and assembled according to the scheme
 shown in Fig. 3: rGO/PEDOT:PSS (poly(styrenesulfonate))/P3HT
 (poly(3-hexylthiophene)):PCBM ([6,6]-phenyl C61-butyric acid
 50 methyl ester)/ TiO_2 /Al. The OPV performance was found to be
 dependent on the charge transport efficiency from the active
 layer to rGO electrode when the optical transmittance of rGO
 was above 65. However, if the transmittance of rGO is less than
 65, the performance of the OPV device is dominated by the light
 55 transmission efficiency, that is, the transparency of rGO films.
 Notably, the substitution of ITO with rGO enhanced the

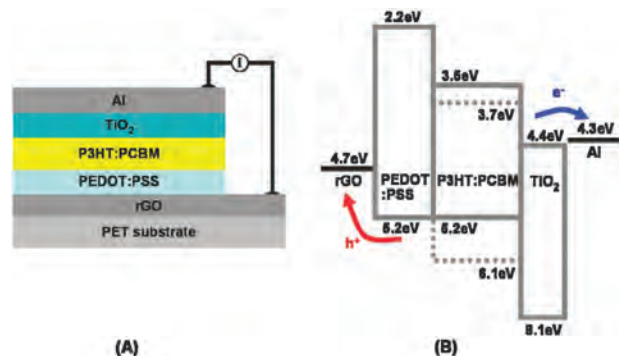


Fig. 3 Schematic representation of (A) the architecture and (B) energy level diagram for the OPV device: rGO/PEDOT:PSS/P3HT:PCBM/ TiO_2 /Al, with an rGO transparent electrode. Reproduced with permission of the American Chemical Society from ref. 18. Copyright 2010.

mechanical flexibility and the performance remained constant
 even after one thousand bending cycles at 2.9 tensile strain.

Graphene TEs have also been successfully applied in DSSCs.
 Müllen and co-workers reported a power conversion efficiency
 (PCE) of 0.26% for the first solid-state DSSC based on a
 graphene electrode fabricated according to graphene/ TiO_2 /
 dye/spiro-OMeTAD/Au.¹⁹ The graphene TEs were prepared by
 dip coating the quartz substrate into an aqueous GO solution,
 followed by temperature-controlled film drying and subsequent
 thermal reduction. The graphene TE exhibited a high conduc-
 tivity of $55\ 000\ \text{S m}^{-1}$ and transparency of more than 70% in the
 wavelength range of 1000–3000 nm.

3.2 Dye-sensitized solar cells

DSSCs have attracted considerable attention as they offer the
 possibility of inexpensive and efficient solar energy conversion.
 In 1991 O'Regan and Gratzel reported a 7% efficient DSSC
 based on nanocrystalline TiO_2 . Subsequent work by Gratzel and
 co-workers demonstrated an efficiency increase to 10% in
 1993.²⁰ While the three major components of the DSSC—dye,
 redox shuttle, and photoanode—have been independently
 investigated over the last 20 years, the most efficient device
 architecture remains largely unchanged from its conception.
 The most prevalent photoabsorbing dyes are ruthenium analogues,
 e.g., $[\text{Ru}(4,4'\text{-dicarboxy-2,2'\text{-bipyridine})}_2(\text{NCS})_2]$ (N_3),
 which absorb incoming photons to form excitons (Fig. 3).
 Excited electrons are rapidly injected into the conduction band
 of TiO_2 and then travel through an external circuit before
 arriving at the counter electrode to reduce I_3^- . Finally, the
 dye is regenerated by I^- .

Many processes can lead to poor photoconversion efficiency
 in DSSCs: the excited state of the dye can decay before it injects
 an electron; the injected electron can recombine with the
 oxidized dye before the dye is regenerated; or the redox shuttle
 can intercept an electron from the photoanode before it is
 collected. Therefore, to improve the PCE of DSSCs, it is crucial
 to maximize the dye loading, the interfacial contact area
 between the dye and electrolyte, and improve the mobility of

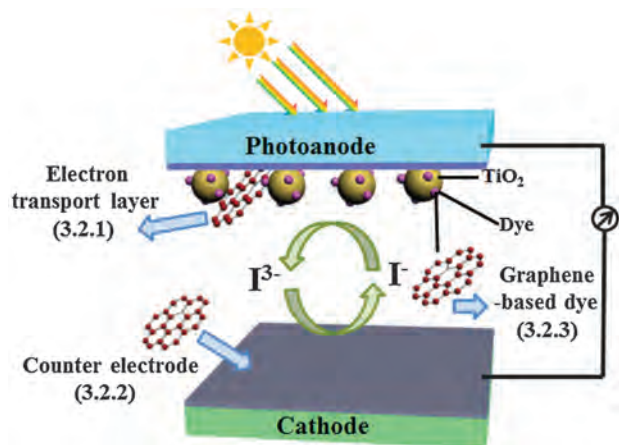


Fig. 4 Device structure of a dye-sensitized solar cell and how graphene is utilized in DSSC to improve the PCE.

electrons at the TiO_2 layer to compete with charge recombination.

In this section, we will talk about utilizing graphene at different parts of DSSC (Fig. 4)—electron transport layer (3.2.1), counter electrode (3.2.2) and dyes (3.2.3), to reduce charge combinations and extend light adsorption range, resulting in a much higher PCE.

3.2.1 Electron transport layer. A major challenge limiting the photoelectric conversion efficiency of DSSCs is the competition between charge transport of photogenerated electrons across the TiO_2 nanoparticle networks and charge recombination within the device. Incorporating graphene into the TiO_2 layer to form an efficient route for charge extraction can significantly suppress recombination and improve charge transport. Yang and co-workers recently showed that graphene- TiO_2 (rGO- TiO_2) composite anodes significantly outperform carbon nanotube- TiO_2 (CNT- TiO_2) anodes in improving the PCE of DSSC due to the 2D electron transport channel created by the graphene sheets (Fig. 5).²¹ In contrast to CNTs that have limited contact with the TiO_2 nanocrystals, graphene

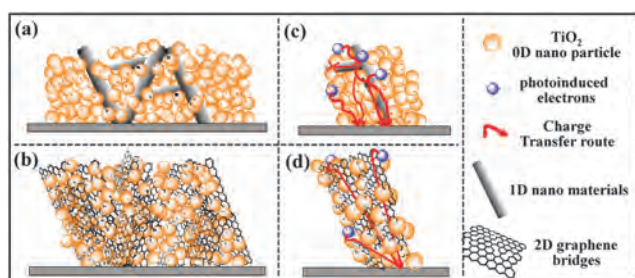


Fig. 5 Differences between 1D (a, c) and 2D (b, d) nanomaterial composite electrodes. For 2D nanomaterial composite electrodes (graphene bridges), the TiO_2 particles adhere to graphene, allowing photoinduced electrons to be removed from the photoanode. For 1D nanomaterial composites, there is less contact between TiO_2 and the 1D nanomaterial; therefore, the transfer is inhibited and recombination is not suppressed. Reproduced with permission of the American Chemical Society from ref. 21. Copyright 2010.

sheets strongly bind to the nanocrystal surface by physisorption and electrostatic interactions to form highly conductive bridges between adjacent TiO_2 particles. The interconnected graphene network acts as an electron transfer medium to rapidly shuttle electrons out of the TiO_2 photoanode, thus suppressing recombination of photogenerated electron-hole pairs (excitons). The short-circuit current density of DSSCs with hybrid rGO- TiO_2 photoanodes increased by 45% without sacrificing the open-circuit voltage, and the photoconversion efficiency reached 6.97%, a 39% increase when compared to pure TiO_2 photoanodes.

The sheet-like structure of graphene has inspired researchers to mimic key light-harvesting structures in photosynthetic organisms. The granum is the core organ in photosynthesis consisting of a stack of ~ 10 – 100 thylakoids containing pigments and electrons acceptors. Fig. 6 shows how stacked structures of TiO_2 -graphene nanosheets can be fabricated in order to mimic the granum core structure.²² The photocurrent of 25 stacked graphene units was found to be 20 times higher than that of pure TiO_2 films. Interestingly, when the number of stacks was greater than 25, the cathodic photocurrent switched to an anodic photocurrent, an important feature of efficient solar cells that is often ignored. By applying principles found in nature to design stacked TiO_2 -graphene structures the photocurrent was shown to significantly increase without sacrificing conductivity.

3.2.2 Catalytic counter electrodes. The platinum counter electrode in DSSCs catalyzes the reduction of I_3^- to I^- after electron injection, thereby recycling the redox shuttle.²⁰ Frustratingly, the reduction of I_3^- can also occur at the surface of

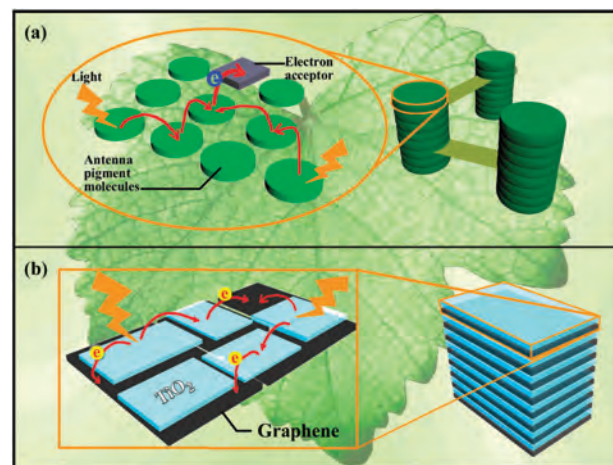


Fig. 6 Real and imitation photosystems with stacked photoanode structures. (a) The granum is composed of stacked thylakoid layers. Antenna pigment molecules absorb light to form excited photoelectrons that are captured and funnelled to the electron acceptor. (b) By imitating the stacked structure of the granum, the stacked structure is composed of alternating layers of TiO_2 and graphene. The enlarged schema shows the TiO_2 acts as the antenna pigment and graphene as the electron acceptor. When many layers are assembled together they form a layered structure akin to what is naturally found in photosynthetic organisms. Reproduced with permission of Wiley from ref. 22. Copyright 2012.

1 TiO₂ nanoparticles, and the competing redox reaction reduces the overall device efficiency. Improving the electrocatalytic efficiency of the counter electrode by inhibiting competing redox reactions is a crucial step toward efficient DSSCs. Due to the rising cost and scarcity of platinum there is a concerted effort to develop efficient counter electrodes using cheaper and earth-abundant materials. Aksay and co-workers have shown graphene can be an inexpensive counter electrode material due to its high conductivity, specific surface area and electrocatalytic activity. Using functionalized graphene sheets (FGSS) as the counter electrode a catalytic efficiency of ~5% was achieved, which is comparative and only 10% lower than platinum counter electrodes.²³ The high catalytic activity was attributed to its comparable charge transfer resistance to platinum under an applied bias, which was induced by active lattice defects and oxygen-containing functional groups in the graphene. Utilizing graphene for counter electrodes in DSSCs is a relatively unexplored area, but it is expected that future breakthroughs will come to reality in graphene surface chemistry and electrode design with decreasing the charge transfer resistance, making it competitive with platinum to ultimately enable the production of low-cost DSSCs.

3.2.3 **Graphene-based dyes.** Discovering an ideal photoabsorbing dye has been a significant challenge and has in part limited the commercialization of DSSCs. Light-absorbing dyes used for DSSCs should possess: (1) a band gap capable of harvesting a majority of the solar spectrum, (2) a conduction band energy that facilitates rapid charge injection to TiO₂, (3) long-term photostability, and (4) good adherence to the TiO₂ surface.²⁰ To date, ruthenium complexes are the most successful dyes and the only to achieve efficiencies over 10%. However, the increasing cost and scarcity of ruthenium inhibit its large-scale application in DSSCs. Pristine graphene is a zero bandgap material, but with chemical functionalization or doping semiconducting properties can be induced, making graphene a promising photoabsorber material for solar cells. Recently, graphene quantum dots consisting of 67 aromatic rings were utilized as the photoabsorber for DSSCs.²⁴ The black-colored graphene quantum dots showed strong absorption up to 900 nm, significantly greater than the standard N719 ruthenium-based dye. The device ultimately had poor performance due to weak interactions between the dye and TiO₂, however, the demonstration is a promising start for the quest to discover cost-effective dyes for DSSCs.

3.3 Organic solar cells

Organic solar cells undoubtedly hold tremendous potential in the photovoltaic market owing to a number of advantageous features, including their thin-film architecture and low material consumption resulting from a high adsorption coefficient, their use of organic materials, which are abundant, their utilization of efficient solution processes and low manufacturing requirements.⁴ Shown in Fig. 7, the prototypical OPV device has a planar layered structure that consists of an organic light-absorbing layer sandwiched between a hole and electron transport layers, and finally two different electrodes that extract

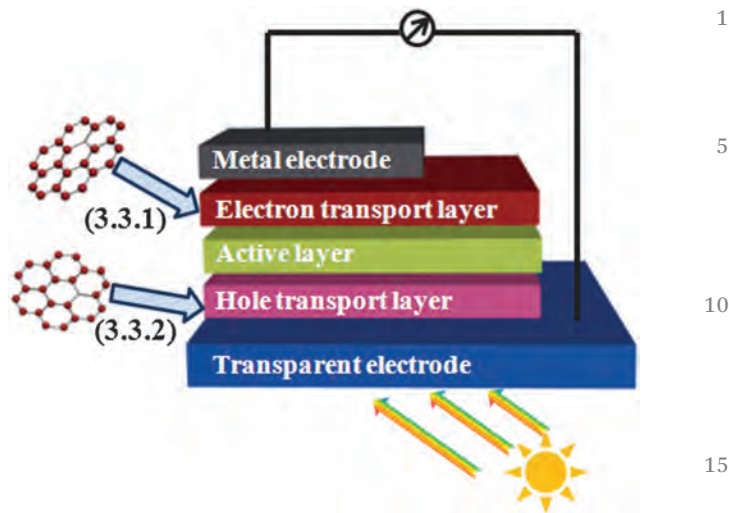


Fig. 7 Device structure of an organic solar cell in the normal configuration and how graphene is utilized in OPV to improve the PCE.

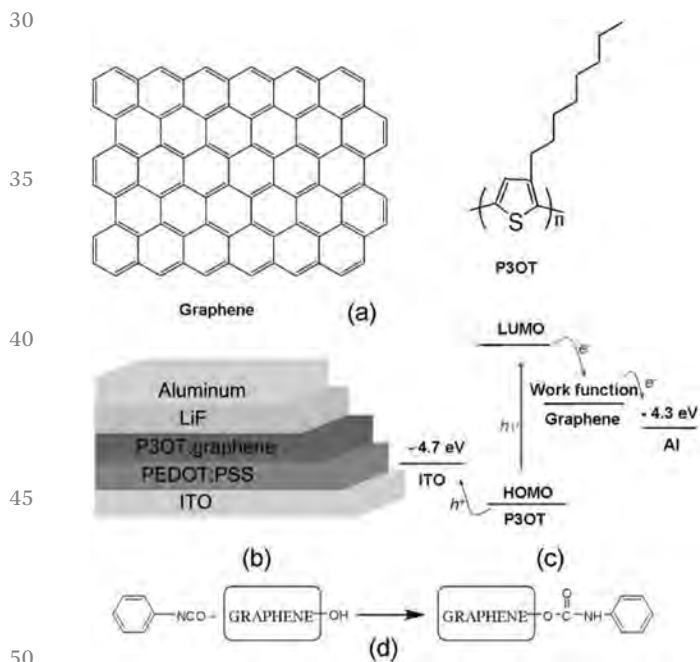
electrons and holes. Light absorption leads to the formation of excitons, or closely bound electron-hole pairs, that dissociate into free electrons and holes at donor/acceptor interfaces before they are transported to opposing electrodes. The electrons in OPVs are collected at a low work function metal electrode (typically aluminium) and holes at the transparent ITO electrode with standard high work function. However, the planar junction concept has certain limitations, including a small surface area between the donor-acceptor interfaces and the requirement of long carrier lifetime to ensure that the electrons and holes reach their respective electrodes. This problem can be addressed by introducing a bulk heterojunction architecture, which involves mixing donor-acceptor materials in the bulk body of an OPV device.²⁵ The representative OPVs with a bulk heterojunction architecture are based on soluble P3HT and poly(3-octylthiophene) (P3OT) as the donor and PCBM as the acceptor and the OPV efficiencies are well above 10%, which indicates remarkable progress towards a promising future. In spite of this, there are many areas for improvement, such as organic-electrode interface engineering since the maximum power conversion efficiencies of OPVs must rise above 15% in the laboratory (corresponding to a module efficiency of around 10–12%) before they can become practically useful.

Graphene has been studied extensively in OPVs in an effort to increase charge transport and overall device efficiency.⁴ Of all graphitic nanomaterials, graphene has the largest conjugated basal plane and is the most amenable for binding to the numerous conjugated polymers found in OPVs. Its work function and bandgap can also be controlled by doping and chemical functionalization, allowing for HOMO (the highest occupied molecular orbital)–LUMO (the lowest unoccupied molecular orbital) matching with conjugated polymers. In addition, graphene is cheap, easily prepared and stable, thus it is expected to be an essential additive for future OPV applications. In this section, attentions are mainly focused on

1 the P3HT-PCBM system to investigate the roles of graphene in
OPV system as electron acceptors (3.3.1) and holes transporters
(3.3.2).

5 **3.3.1 Electron transporters and acceptors.** A vital aspect of
polymer-based OPVs is the electron donor/acceptor interface
between the photoabsorbing polymer (*e.g.*, P3HT) that gener-
ates excitons and the acceptor layer that dissociates the exci-
tons and extracts electrons. Fullerene derivatives (*e.g.*, PCBM)
10 are among the most effective acceptors due to their high
electron affinity and charge mobility, which represents a mile-
stone in the development of OPV acceptors and is still widely
used today. The combination of P3HT and PCBM has been
studied extensively in various configurations; however, electron
15 transport at the heterojunction is hindered due to challenges
associated with polymeric phase separation, such as isolated
polymer domains and structural traps.

When blended with conjugated polymers, graphene can
enhance electron-hole separation and charge transport by
providing a continuous pathway for electronic extraction,
20 owing to its large surface area that improves interfacial
donor/acceptor contact. For example, Chen and co-workers
showed that functionalized graphene serves as a competitive
alternative to PCBM as the electron acceptor for OPV devices. By
blending functionalized graphene with P3HT in a bulk hetero-
25 junction OPV they achieved a power-conversion efficiency of
1.4% with a graphene content of 10 wt% (Fig. 8).²⁶ By thermal
annealing, the functional groups from the graphene were

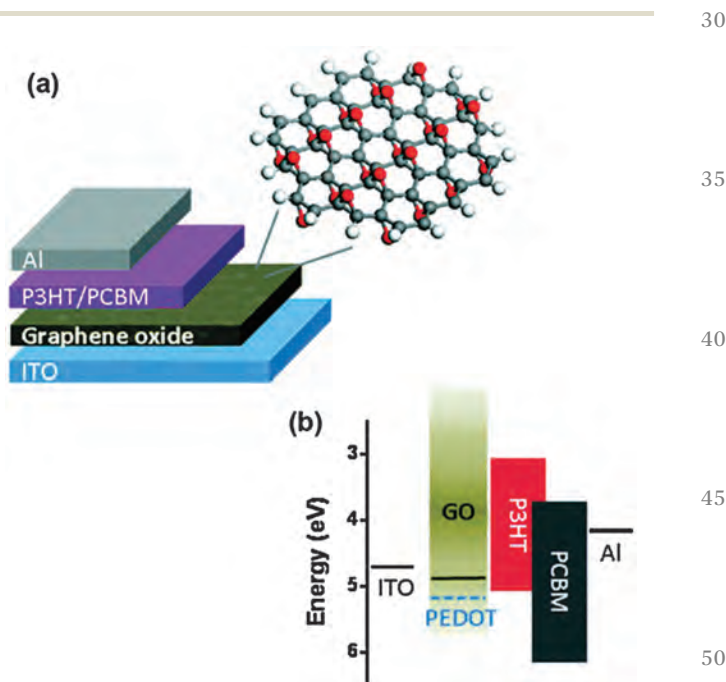


30
35
40
45
50
55
Fig. 8 (a) The idealized chemical structures of graphene and P3OT. (b) Schematic of the device with P3OT-graphene thin film as the active layer and the structure ITO (ca. $17 \Omega \text{ sq}^{-1}$)/PEDOT:PSS (40 nm)/P3OT: graphene (100 nm)/LiF (1 nm)/Al (70 nm). (c) Energy level diagram of P3OT and functionalized graphene. (d) Schematic representation of the reaction of phenyl isocyanate with graphene oxide to form functionalized graphene. Reproduced with permission of Wiley from ref. 26. Copyright 2008.

removed and the crystallinity of P3OT improved. The great
improvement in performance was attributed to the well-
dispersed percolated graphene network that facilitated charge
separation and transport.

5 **3.3.2 Hole transport layers.** Hole transport layers situate
between the ITO anode and the electron donor/acceptor layer
and prevent excitons recombination and current leakage in
OPVs.⁴ The most common hole transport materials PEDOT:PSS
align the work functions of P3HT and ITO for more efficient
10 hole collection, and also eliminate the propagation of ITO
roughness through the device. However, PEDOT:PSS is typically
deposited from highly acidic ($\text{pH} \sim 1$) aqueous solutions that
are known to incorporate water into the active layer and corrode
ITO at elevated temperatures, both of which degrade device
15 performance.

Graphene oxide has been demonstrated as simple and
effective alternative to PEDOT:PSS hole transport layers in
polymer-based OPVs. Li and co-workers showed the addition
of a 2 nm-thickness graphene oxide film between ITO and
P3HT:PCBM reduced excitonic recombination and leakage
20 current, resulting in a substantial increase in short circuit
current density (J_{sc}), open-circuit voltage (V_{oc}), and fill factor
(FF), and a power conversion efficiency of $3.5 \pm 0.3\%$ was
achieved, which is comparable to devices with PEDOT:PSS hole
transport layers (Fig. 9).²⁷ These results, combined with the
25 promising work using graphene transparent electrodes and
electron transport/acceptors provide the basis for the develop-
ment of OPVs based on an all-carbon platform.



30
35
40
45
50
55
Fig. 9 (a) Schematic illustration of OPV device with a GO hole transport layer, assembled with the following architecture: ITO/GO/P3HT:PCBM/Al. (b) Energy level diagrams of the ITO electrode, interlayer materials (PEDOT:PSS, GO), P3HT (donor), and PCBM (acceptor), and top Al electrode. Reproduced with permission of the American Chemical Society from ref. 27. Copyright 2010.

3.4 Quantum dot solar cells

Quantum dot (QD) based solar cells are poised to play a leading role in providing scalable and inexpensive solar energy, owing to their size-tunable optical response, solution processability, and ability to exceed the Shockley–Queisser limit (33.7%) through multi-exciton generation. However, charge extraction of photogenerated excitons from the QD absorber layer remains a major challenge in developing high-performance QD solar cells. Incorporating graphene into QD-based PVs has shown to be a promising approach to minimize excitons recombination and enhance photocurrent without significantly affecting production costs.

Guo and co-workers reported a QD-based PV with graphene–QD composites as electron absorber layer that graphene was utilized as an electron acceptor additive.²⁸ The IPCE (monochromatic incident photon-to-electron conversion efficiency) reached an impressive 16% while the photoresponse was 1.08 mA cm⁻² under light illumination of 100 mW cm⁻², which is the best performance of all reported carbon–QD solar cells. The marked improvement in photoconversion efficiency and photocurrent demonstrate that graphene is a promising candidate for enhancing the charge collection in QD-based solar cells.

However, graphene sheets are prone to aggregate in certain applications and have limited dispersability in common solvents. This problem has recently been addressed by the advent of graphene quantum dots (GQDs), the 0D analogue of 2D graphene sheets. GQDs have pronounced quantum confinement effects and show size-dependent photoluminescent properties. They display low cytotoxicity, excellent solubility, stable photoluminescence, and are easily functionalized, making them applicable in many technologies such as optoelectronic devices, sensors, and fluorescent probes for bioimaging.

Recently, Li and co-workers reported the synthesis of stabilized GQDs with uniform and tunable size by covalently attaching multiple 2',4',6'-trialkyl phenyl groups to the edges of small graphene sheets.²⁴ The GQDs consist of graphene moieties containing 168, 132 or 170 conjugated carbon atoms, respectively. Optical characterizations indicate the GQDs absorb a wide spectrum of light across visible and near IR regions, with a maximum at 591 nm. GQD-sensitized solar cells fabricated using an architecture analogous to the structure of a DSSC showed a short-circuit current density of 200 μA cm⁻², an open-circuit voltage of 0.48 V, and a fill factor of 0.58, which are comparable figures of merit to devices sensitized by ruthenium complexes.

Green-luminescent water-soluble GQDs with diameter of about 3–5 nm have also been synthesized by an electrochemical approach. OPVs fabricated with a hybrid P3HT-GQD electron-acceptor layer have achieved a power conversion efficiency of up to 1.28% (Fig. 10).²⁹ In this configuration, the GQDs effectively dissociate excitons and transport carriers out of the absorber layer to the aluminium cathode.

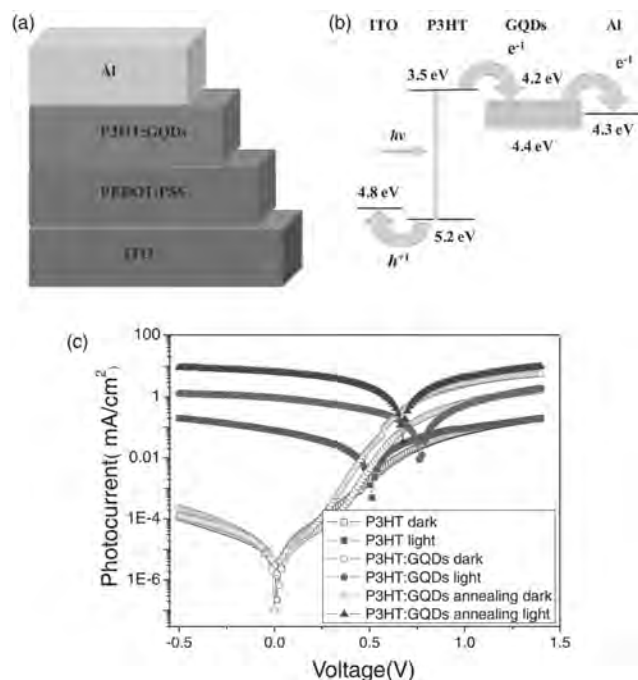


Fig. 10 Schematic (a) and energy band diagrams of the ITO/PEDOT:PSS/P3HT:GQDs/Al device. (c) J - V characteristic curves for the ITO/PEDOT:PSS/P3HT/Al, ITO/PEDOT:PSS/P3HT:GQDs/Al and ITO/PEDOT:PSS/P3HT:GQDs/Al devices after annealing at 140 °C for 10 min, single log scale. Reproduced with permission of Wiley from ref. 29. Copyright 2011.

4. Photocatalytic applications of graphene

Since the discovery of the photocatalytic water splitting with TiO₂ electrodes by Fujishima and Honda in 1972, there have been tremendous advances in the areas of photocatalytic solar energy conversion, environmental decontamination, and generation of solar fuels.³⁰ Photocatalysts are typically wide band-gap semiconductors (*e.g.*, TiO₂; $E_g = 3.2$ eV; 388 nm) that form excitons upon light illumination. However, unlike in solar cells, the photogenerated holes and electrons are not collected at the electrodes but quickly scavenged at the surface by adsorbed molecules for photocatalytic reactions. The surface reactions can range from the conversion of H₂O to H₂ and O₂, to the transformation of organic pollutants to CO₂ and H₂O, among others. Generally, there are three fundamental approaches for enhancing the photocatalytic activity and applicability of semiconductor photocatalysts: (i) bandgap tuning and/or extension of excitation wavelength with photosensitizers, (ii) minimizing charge carrier recombination, and (iii) promotion of the forward reaction and surface adsorption by increasing the number of active surface sites.

Carbon nanomaterials, such as activated carbon, carbon nanotubes and fullerenes, have been studied extensively for various photocatalytic applications due to their promising electronic and catalytic properties. However, graphene has

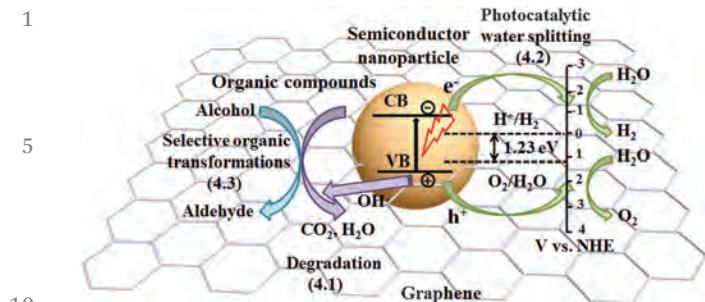


Fig. 11 Schematic illustration of graphene-enhanced photocatalysis, including degradation (4.1), photocatalytic water splitting (4.2) and selective organic transformation (4.3).

been demonstrated as the preminent carbon nanomaterial for enhancing photocatalytic performance of semiconductors. High-quality graphene sheets permit ballistic transport, meaning electrons can travel unobstructed at mobility exceeding $\sim 20\,000\text{ m}^2\text{ V}^{-1}\text{ s}^{-1}$ at room temperature, making them ideal electron sinks or electron bridges for transferring excitons to surface adsorbed molecules. Also graphene has a theoretical surface area of up to $2600\text{ m}^2\text{ g}^{-1}$, making it an attractive high surface area 2D photocatalyst support with a high density of reactive adsorption sites. Furthermore, the one-atom-thick structure provides high transparency.

This section provides an overview of graphene-based photoactive nanocomposites utilized for environmental remediation and energy conversion, including photodegradation of organic compounds (4.1), water splitting (4.2), and selective organic transformations (4.3) (Fig. 11).

4.1 Degradation of organic compounds

Rampant industrial pollution has become a serious threat to human beings and there is a global push to remove toxic organic pollutants from the atmosphere, municipal water supplies, and compromised ecosystems. Semiconductor photocatalysts such as TiO_2 , ZnO , CdS , ZnS , and their derivatives, are considered among the most promising candidates for photocatalytic degradation of organic pollutants as they purify contaminated fluids with only sunlight, and without the production of harmful by-products.³⁰ However, their relative low photocatalytic activity and inefficient utilization of the solar spectrum limit their practical use. Graphene has been widely used to enhance the photocatalytic properties of semiconductors due to its high adsorption capacity for organic molecules, ability to modify the bandgap of semiconductors to extend the light absorption range, and enhance charge separation and transportation. Graphene-semiconductor photocatalytic hybrid nanomaterials have been investigated extensively for environmental remediation and disinfection purposes.

Lightcap and co-workers were one of the first to demonstrate the ability of graphene to extract excitons from TiO_2 and store electrons for subsequent photocatalytic reactions (Fig. 12).³¹

Fig. 12B shows that dispersions of TiO_2 nanocrystals change from clear to blue upon illumination, indicating the formation

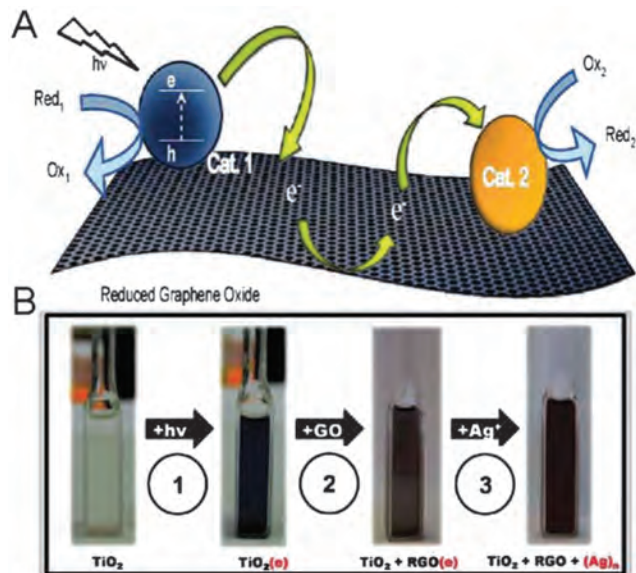


Fig. 12 (A) Schematic illustration of selective catalysis at different sites on rGO, and (B) photographs showing the color changes observed during stepwise electron transfer and reduction of Ag^+ : ① excitation and storing electrons in TiO_2 by irradiating air-free ethanol suspensions with UV light ($\lambda > 300\text{ nm}$) for 30 min; ② addition of air-free ethanol suspension of GO until no blue colour remains (gray colour due to the presence of rGO); ③ reduction of Ag^+ to Ag nanoparticles (red colour) by stored electrons in rGO following the addition of air-free AgNO_3 solution. Reproduced with permission of the American Chemical Society from ref. 31. Copyright 2010.

of trapped excitons. Upon addition of graphene oxide, the blue color disappears as a result of its reduction to reduced graphene oxide. During this process, approximately 16% of the initially trapped excitons are stored in the surface of reduced graphene oxide and are available for electrochemical reduction. When successive and controlled amounts of AgNO_3 solution were added under no further illumination, Ag^+ was readily reduced to Ag nanoparticles anchored on graphene sheets, resulting in the formation of ternary nanocomposites. This phenomenon provides strong evidence for the ability of graphene to store electrons for further electrochemical reduction reactions (Fig. 12A).

While TiO_2 shows excellent photocatalytic activity and chemical stability, its wide bandgap ($E_g = 3.2\text{ eV}$) requires activation by high energy UV irradiation that comprises only about 5% of the solar spectrum. Visible-light responsive photocatalysts could be more ubiquitously applied in commercial or industrial applications, but are challenging to design and produce. Recently, TiO_2 -graphene oxide and TiO_2 -graphene composites have shown to undergo visible-light photocatalysis. As evidence, Zhang and co-workers reported the visible-light driven photocatalytic degradation of methylene blue using hydrothermally synthesized TiO_2 -graphene oxide composites.³² The photocatalytic activity of the composite was found to be much greater than bare TiO_2 nanocrystals under UV and visible illumination. The photocatalytic enhancement was attributed to: (1) graphene-induced narrowing of the TiO_2 band gap *via* the formation of Ti-O-C bonds that extends the photoresponse

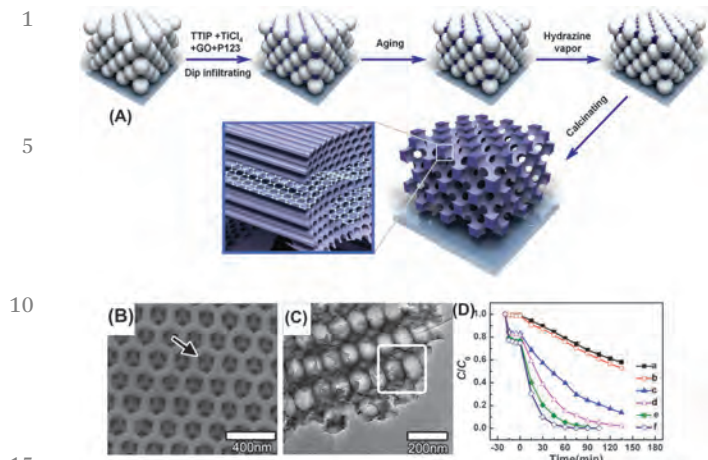


Fig. 13 (A) Illustration of the preparation of macro-mesoporous TiO_2 -graphene composite films; (B) typical SEM and (C) TEM images of macro-mesoporous TiO_2 -graphene composite films assembled using 300 nm polystyrene sphere templates; (D) photocatalytic degradation of methylene blue under UV light irradiation ($\lambda = 365$ nm) using (a) Ti-Me, (b) graphene-Ti-Me, (c) Ti-Ma200-Me, (d) graphene-Ti-Ma200-Me, (e) Ti-Ma170-Me, and (f) graphene-Ti-Ma170-Me films. Reproduced with permission of the American Chemical Society from ref. 33. Copyright 2011.

into the visible region, (2) suppression of exciton recombination by rapid electron extraction from TiO_2 to the graphene surface, and (3) enhanced adsorption of organic molecules onto the graphene surface.

Incorporating graphene into the synthesis of macro/mesoporous TiO_2 has shown to be an excellent method for guaranteeing interfacial contact and improving photocatalytic performance. Du and co-workers demonstrated the formation of TiO_2 -graphene hierarchically ordered macro-mesoporous composite films *via* a self-assembly method.³³ As illustrated in Fig. 13A, macro-mesoporous TiO_2 -graphene composite films were prepared by adding graphene oxide to an array of self-assembled polystyrene spheres, followed by an *in situ* reduction. The aqueous photocatalytic activity was evaluated by the degradation rate of methylene blue. Fig. 13D demonstrates that the photodegradation rate constants for macro-mesoporous TiO_2 films without and with graphene were almost 11 and 17 times higher than those for traditional mesoporous TiO_2 films, respectively. The hierarchically ordered macro-mesoporous film structure improves mass transport through the film, reduces the mesopore channel length, and increases the accessible catalytically active sites within the film. The incorporation of graphene into the framework effectively enhances photocatalytic activity by suppressing charge recombination and more efficiently utilizing photogenerated electrons for catalysis.

Graphene has widely been used to enhance the photocatalytic disinfection, protect biomolecules from enzymatic cleavage. Akhavan and co-workers reported the antibacterial activity of graphene- TiO_2 thin films against *E. coli* bacteria under solar light irradiation.³⁴ The photocatalytic reduction of graphene oxide platelets under UV irradiation can destroy

99.9% *E. coli* bacteria in 4 h with an enhance factor of about 7.5 towards the TiO_2 thin film. The mechanism of photocatalytic decontamination involves the generation of reactive oxygen species (ROSS) such as hydrogen peroxide (H_2O_2), $\cdot\text{OH}$, and $\cdot\text{O}_2^-$ that form at the composite surface under UV light. ROSS generated from graphene oxide- TiO_2 have also been utilized for photodynamic cancer therapy, where cell death occurs when ROSS disrupt cellular membranes and internal organelles.

4.2 Photocatalytic water splitting

Using solar energy to split water is the cleanest and most idealistic route for producing H_2 , a clean burning carbon-free fuel. Conversion from carbon-based fossil fuels to H_2 generated by carbon-neutral processes has the potential to curb the perpetual demand for energy, without contributing to the enhanced greenhouse effect and global warming.³⁰ In practice, however, the large-scale conversion of sunlight to solar fuel is limited by the availability of stable and efficient photocatalysts that utilize visible light. For a single semiconductor to split water and simultaneously produce H_2 and O_2 —by providing electrons to reduce H^+ to H_2 and holes to oxidize H_2O to O_2 —it must have a bandgap greater than 1.23 eV and valence and conduction bands that straddle the water-splitting potential. Fig. 11 shows the bottom of the conduction band must be above the redox potential of H^+/H_2 (0 V vs. NHE), while the top of the valence band must be below the redox potential of $\text{O}_2/\text{H}_2\text{O}$ (1.23 V).³⁵ Very few semiconductors have the electronic properties to satisfy these stringent requirements. For instance, CdS has a bandgap of 2.4 eV and satisfies the electronic requirements for a visible light water splitting photocatalyst, however, challenges associated with electrode corrosion during operation restrict its utility. TiO_2 on the other hand straddles the water splitting potential and is very stable in aqueous systems; however, it also has its limitations. It has a bandgap in the UV region and its conduction band level is relatively positive, resulting in very little driving force for the production of H_2 . As a result, a co-catalyst such as platinum is commonly combined with TiO_2 in order to increase the rate of H_2 production. In addition, slow electron transfer and exciton recombination reduces the efficiency, or quantum yield of TiO_2 . By utilizing graphene as an efficient electron acceptor and transporter, researchers have improved the photocatalytic activity of semiconductors for the production of H_2 .

The effectiveness of graphene as an electron acceptor and transporter is highly dependent on the interfacial contact between graphene and TiO_2 , which relates to the design and production of TiO_2 -graphene composites. Fan and co-workers compared the H_2 production efficiency from P25 (Aeroxide TiO_2)-rGO composites prepared by UV-assisted photocatalytic reduction, hydrazine reduction, and hydrothermal synthesis.³⁶ Among them, the P25-rGO composites prepared by hydrothermal synthesis showed the best performance—for P25/rGO with a mass ratio of 1.0/0.2 the hydrogen evolution rate was $74 \mu\text{mol h}^{-1}$, one order of magnitude higher than that for P25 alone (H_2 : $6.8 \mu\text{mol h}^{-1}$). The composites even showed catalytic H_2 evolution in pure water without the need for sacrifice agents. It was

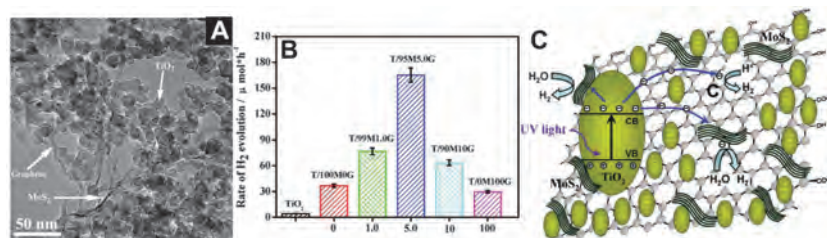


Fig. 14 (A) TEM image of TiO₂-MoS₂-rGO composite. (B) Photocatalytic H₂ evolution for TiO₂/MoS₂/rGO co-catalysts under UV irradiation containing varying ratios of MoS₂ and rGO. (C) Schematic illustration of the charge transfer process in TiO₂-MoS₂-rGO composites during illumination. Reproduced with permission of the American Chemical Society from ref. 37. Copyright 2012.

proposed that the hydrothermal method provided the most intimate contact between the P25 and rGO, allowing the composites to fully take advantage of the electron acceptor/transporter ability of graphene.

Co-catalysts of MoS₂-graphene composites have also shown to greatly enhance H₂ production by suppressing charge recombination, improving interfacial charge transfer, and providing a large number of photocatalytical active reaction sites. Fig. 14C shows the synergistic effects of MoS₂ and rGO in TiO₂-MoS₂-graphene composites which yield an H₂ production rate of 165.3 μmol h⁻¹, with an impressive quantum efficiency of 9.7% at 365 nm.³⁷ For this example, the content of MoS₂-graphene co-catalyst in the composite was 0.5 wt%, of which graphene was only 5.0 wt%.

Among the various visible-light-driven photocatalysts for H₂ production, CdS is a particularly attractive material because its narrow bandgap of 2.4 eV that straddles the water splitting potential. Unfortunately, CdS suffers from low exciton separation efficiency and photocorrosion during light irradiation. Li and co-workers increased exciton separation and transport efficiency for visible-light-driven photocatalysis by producing graphene nanosheets decorated with CdS clusters.³⁸ Fig. 15 shows the nanocomposites composed of 1.0 wt% graphene and 0.5 wt% platinum attain H₂ production rates of 1.12 mmol h⁻¹ (about 4.87 times higher than that of pure CdS nanoparticles) under visible light irradiation at 420 nm. The advantageous electron extraction and storage capabilities of graphene have also been employed to enhance the photocatalytic H₂

production of other visible-light-active semiconductors, such as graphitic carbon nitride (g-C₃N₄), Ru-SrTiO₃:Rh, BiVO₄, and ternary hybrids system of graphene and semiconductors.³⁵

Photoelectrochemical cells (PECs) offer a possibility to split water by using an applied bias for semiconductor photoanode composites with bandgaps less than 1.23 eV or conduction band level mismatches the reduction potential of H⁺/H₂. The external bias is necessary for H₂ production as it partially depletes electrons in the photoactive materials, reduces recombination and increases the lifetime of photogenerated charges. Hou and co-workers reported a PEC based on a heterojunction array of α-Fe₂O₃-graphene-BiV_{1-x}Mo_xO₄ core-shell nanorods that reached a maximum photoconversion efficiency of 0.53% at -0.04 V (0.56 V vs. NHE), which is considerably higher than Fe₂O₃/rGO or Fe₂O₃ alone (Fig. 16).³⁹ The PEC was composed of a working photoanode (α-Fe₂O₃/graphene/BiV_{1-x}Mo_xO₄) for O₂ evolution, a platinum counter photocathode and an electrolyte containing an electron donor additive. The authors proposed that forming a heterojunction between Fe₂O₃/rGO and BiV_{1-x}Mo_xO₄ shifted the Fermi level of the composite so that the band difference between the Fermi levels of Fe₂O₃ and BiV_{1-x}Mo_xO₄ lead to the shifts of their energy bands until their Fermi levels reached equilibrium. Upon irradiation, photo-generated holes and electrons appeared in the VB and CB of Fe₂O₃ and BiV_{1-x}Mo_xO₄, respectively. Thanks to the band alignment and potential difference, rGO sheets as an excellent electron conductor provided a direct pathway for electrons to transfer from the CB of BiV_{1-x}Mo_xO₄ shell to the CB of Fe₂O₃ core easily. The

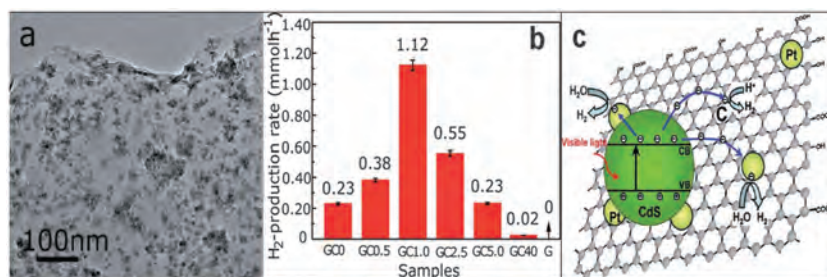


Fig. 15 (a) TEM image of CdS-graphene composite (1 wt% graphene, denoted as GC1.0); (b) comparison of the visible-light photocatalytic activity of GC0, GC0.5, GC1.0, GC2.5, GC5.0, GC40, and rGO for the production of H₂ in solutions containing 10 vol% lactic acid and a 0.5 wt% Pt co-catalyst. (c) Schematic illustration of the charge separation and transfer in the CdS-rGO system under visible light. Reproduced with permission of the American Chemical Society from ref. 38. Copyright 2011.

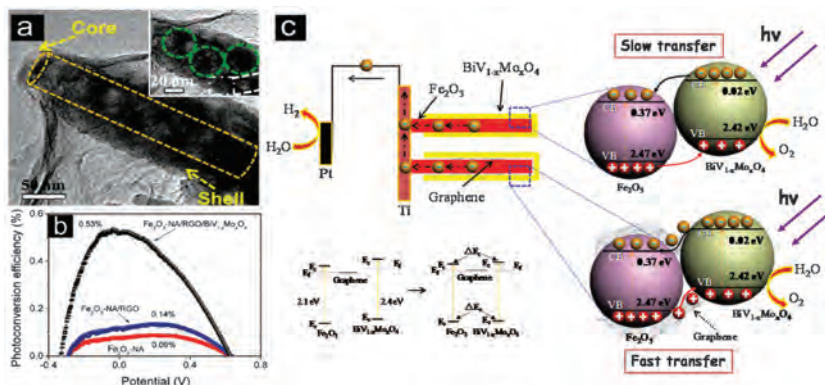


Fig. 16 (a) TEM image of Fe₂O₃-NA (nanorod array)/rGO/BiV_{1-x}Mo_xO₄ heterojunction; (b) photoconversion efficiency as a function of applied potential for Fe₂O₃-NA, Fe₂O₃-NA/rGO, and Fe₂O₃-NA/rGO/BiV_{1-x}Mo_xO₄ heterojunction in 0.01 M Na₂SO₄ solution under Xe lamp irradiation; (c) schematic for the energy band structure of the Fe₂O₃-NA/rGO/BiV_{1-x}Mo_xO₄ heterojunction and proposed mechanism of photoelectrochemical water splitting. Reproduced with permission of the American Chemical Society from ref. 39. Copyright 2012.

electrons in Fe₂O₃ then migrated to the Ti substrate along the Fe₂O₃ nanorods, and ultimately transferred to the Pt electrode for H₂ evolution by reducing water under the external electrostatic field. Simultaneously, the holes in the VB of Fe₂O₃ which migrated to the VB of BiV_{1-x}Mo_xO₄ *via* the rGO interlayer would be consumed by oxidizing water to form O₂. Thus, the photo-induced charges were efficiently separated, resulting in the enhancement of PEC activity.

Graphite oxide can also serve as a photocatalyst for hydrogen production when oxidized to an appropriate extent.⁴⁰ H₂ generation can occur when the CB minimum of GO is greater than -0.52 eV (vs. NHE, pH = 0), while the VB maximum of GO mainly varies with the degree of reduction. Considering the bandgap of GO decreases with the increasing extent of reduction, tailoring the level of GO can provide a material with an appropriate bandgap for water splitting. Graphene has also been observed as photosensitizer in visible-light-driven photocatalytic water splitting, such as in rGO-TiO₂ and rGO-ZnO composites where it serves to transfer photoexcited electrons from graphene to semiconductor.³⁵ The mechanism can be explained as follows: electrons in the HOMO of graphene are excited to the LUMO of graphene under visible light irradiation, and these photoinduced electrons are injected to the CB of semiconductor. The reduction reaction subsequently occurs at the surface of the semiconductor, all under visible light initiation.

4.3 Selective photocatalytic chemical transformations

Photocatalytic reactions are commonly thought to be unselective, yet recent progress indicates that photocatalysis can serve as an alternative to conventional synthetic production of fine chemicals. A majority of the photocatalytic applications of graphene-based nanocomposites often focus on non-selective chemical transformations. However, by selecting appropriate photocatalysts and controlling reaction conditions, selective organic transformations are attainable. Xu and co-workers reported the selective oxidation of alcohols to aldehydes with O₂ using graphene-TiO₂ nanocomposites under mild

conditions.⁴¹ Upon visible light irradiation, alcohols were transformed to aldehydes with a high yield and selectivity. When compared to CNT-TiO₂, the graphene-TiO₂ composites showed better charge separation, higher photocatalytic activity and selectivity for the transformation of alcohols to aldehydes. This was attributed to the superior interfacial contact between the graphene and TiO₂ of nanocomposite. These promising results demonstrate the potential role of graphene composites in the photocatalytic production of fine chemicals, in addition to advancing graphene-semiconductor nanocomposites for artificial photosynthesis.

5. Graphyne and graphdiyne: new 2D members of the carbon family

5.1 Graphyne

Graphyne was first predicted by Baughman and co-workers in 1987 and is composed of planar sheets occupied equally by sp² and sp carbon atoms.⁴² Shown in Fig. 17, this 2D allotrope of carbon can be visualized as sheets of benzene rings connected by acetylene bonds and comes in various forms, such as α -graphyne, β -graphyne and 6,6,12-graphyne.⁴³ Depending on the acetylene content graphyne has a mixed hybridization (spⁿ, where 1 < n < 2), and thus differs from graphene (purely sp²) and diamond (purely sp³). Graphyne has yet to be synthesized in the laboratory, but its structure and electronic properties have been predicted with the use of computer models.

Thermodynamics calculations predict graphyne to have crystalline-state formation energy of 12.4 kcal mol⁻¹, much lower than any other carbon phase that contains acetylenic groups as major structural components.⁴⁴ The isolated planar sheets have the identical symmetry as graphene (*p6m*) and the theoretical unit cell of graphyne contains two sheets and overall lattice constants of *a* = 6.86 Å, *c* = 6.72 Å, and γ = 120°. Graphyne is also predicted to have similar thermal stability and mechanical properties to graphite.

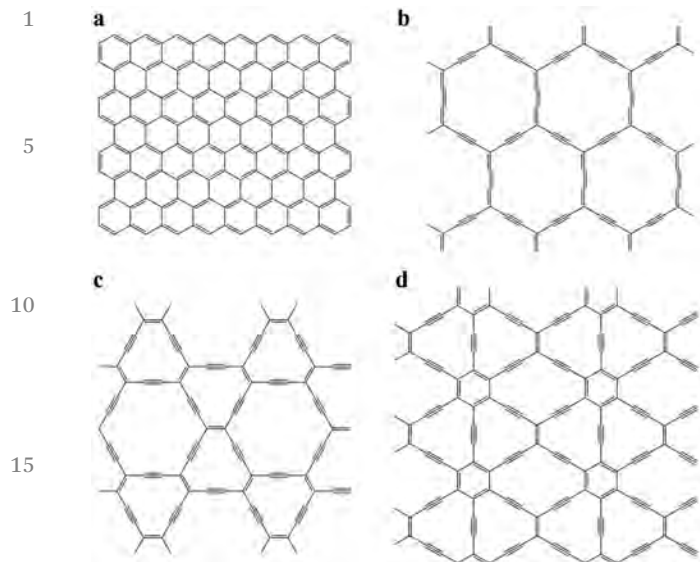


Fig. 17 Structures of graphene and graphynes. (a) Graphene, (b) α -graphyne, (c) β -graphyne, (d) 6,6,12-Graphyne. Reproduced with permission of the American Physical Society from ref. 43. Copyright 2012.

The excitement surrounding graphyne is predominantly related to its potential for never-before-seen electronic transport properties. Graphyne is predicted to be a direct-bandgap semiconductor with a gap energy of about 1.2 eV, and two self-doped non-equivalent distorted Dirac cones. To understand this concept, the outstanding electronic properties of graphene similarly arise from its unique band structure where the honeycomb lattice (a hexagonal lattice with two equivalent atoms per unit cell) creates six points in reciprocal space where the valence and conduction bands meet at the Fermi level, leading to zero effective mass for electrons and holes and impressive room temperature electron mobility of up to $20\,000\text{ cm}^2\text{ v}^{-1}\text{ s}^{-1}$. The presence of Dirac cones was previously thought to only occur in graphene, however, recent DFT (density functional theory) band structure calculations by Görling and co-workers showed Dirac cones exist in all three forms of graphyne— α -graphyne, β -graphyne and 6,6,12-graphyne (Fig. 17b–d), revealing the fact that all carbon atoms are chemically equivalent in graphene is not a prerequisite for the existence of a Dirac cone and the accompanying electronic properties, like outstanding conductivity.⁴³ Especially 6,6,12-graphyne, which have a rectangular symmetry, is predicted to have two different Dirac cones lying slightly above and below the Fermi level, implying it intrinsically a self-doped semiconductor in the sense that at one Dirac cone electrons are present as charge carriers while at the other Dirac cones holes are present as charge carriers, offering the possibility for directional-dependent electronic properties. This would be a distinct advantage over graphene, which has isotropic in-plane electronic properties in this ideal form and requires external doping to enable semiconducting properties.

5.2 Graphdiyne

Graphdiyne (GD) is currently the most synthetically attainable analogue of graphyne. Proposed by Haley and co-workers, GD is a 2D carbon allotrope containing planar sp and sp^2 carbon atoms, but differs from graphyne in its structure that contains two acetylenic diacetylenic linkages between carbon adjacent hexagons.⁴⁵ With a heat of formation of 18.3 kcal per g-atom C, GD is the most stable carbon allotrope containing diacetylenic linkages and is anticipated to exhibit fascinating properties such as third-order nonlinear optical susceptibility, excellent conductivity or superconductivity (when doped with alkali metals), and enhanced redox activity. Complex DFT performed by Long and co-workers showed that GD sheets have semiconductor properties with a band gap of 0.46 eV and an in-plane electron mobility on the order of $10^5\text{ cm}^2\text{ V}^{-1}\text{ s}^{-1}$ at room temperature, with a hole mobility about an order of magnitude lower.⁴⁶ GD nanoribbons showed similar electron mobility ($10^4\text{ cm}^2\text{ V}^{-1}\text{ s}^{-1}$) but significantly lower hole mobility due to strong acoustic phonon scattering.

Very recently large area ($\sim 3.6\text{ cm}^2$) graphdiyne films were successfully synthesized by Li and co-workers on the surface of copper *via* a cross-coupling reaction using hexaethynyl benzene in the presence of pyridine (Fig. 18).⁴⁷ Similar to vapor phase synthesis of graphene, copper served as both the catalyst and substrate for growing GD films. Fig. 18 shows the flexible GD films were about $1\text{ }\mu\text{m}$ thick and composed of multilayers. HRTEM (high-resolution transmission electron microscope) images reveal that the GD films do not contain defects or dislocations, and clear lattice spacings of $4.19\text{ }\text{\AA}$ are observed, which are considerably larger than that of graphene ($2.32\text{ }\text{\AA}$) or graphite ($2.46\text{ }\text{\AA}$). Selective area electron diffraction and XRD (X-ray diffraction) patterns confirm the GD is highly crystalline. GD devices fabricated on Cu foils exhibited Ohmic behavior with calculated conductivities of $2.516 \times 10^{-4}\text{ S m}^{-1}$, which is comparable to silicon. These promising electronic properties

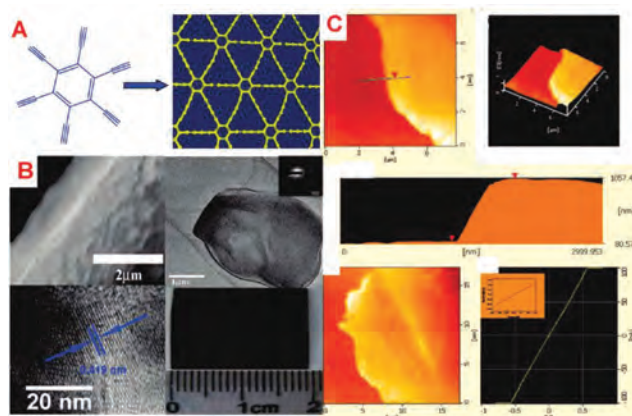


Fig. 18 (A) Schematic representation of a graphdiyne monomer and a corresponding nanoscale film, (B) SEM, TEM, HRTEM, and photographic images of a large area graphdiyne film, and (C) AFM images and the corresponding I - V curve. The inset is the I - V curve of graphdiyne films measured on the device. Reproduced with permission of the Royal Society of Chemistry from ref. 47. Copyright 2010.

1 demonstrate the potential of GD in solid-state or flexible
electronic device applications, photoelectrical conversion and
photocatalysis.

OPVs containing electron transport layers of GD doped
5 P3HT:PCBM were fabricated by Li and co-workers and exhib-
ited an enhanced J_{sc} of 2.4 mA cm^{-2} and an impressive PCE of
3.52%, which is 56% higher than that without GD doping.⁴⁸
Similar to the effects of graphene, the improved cell perfor-
10 mance is attributed to excellent charge transfer capability of GD
and the formation of percolated paths to extract electrons from
the absorber layer.

The large surface area and high electron mobility of GD has
also been utilized to improve the photocatalytic activity of TiO_2
for the degradation of organic molecules. Wang and co-workers
15 prepared nanocomposites of P25 and GD (P25-GD) by a facile
hydrothermal method and demonstrated a 4.5% increase in the
photocatalytic degradation of methylene blue at an optimized
ratio of 0.6 wt% (Fig. 19).⁴⁹ The P25-GD composites also show
considerable visible-light-driven photocatalytic activity due to
20 the formation of chemical bonds between TiO_2 and GD that
effectively narrows the bandgap of P25 and extends light
absorption range into the visible region.

To compare the relative photocatalytic enhancement of
graphene and GD, Yang and co-workers monitored the photo-
25 catalytic degradation rates of methylene blue with TiO_2 -GD and
 TiO_2 -graphene nanocomposites.⁵⁰ Fig. 20 shows the degrada-
tion rate constant of methylene blue when the TiO_2 -GD compo-
site is 1.63 ± 0.15 times that of the pure TiO_2 , and $1.27 \pm$
0.12 times that of the TiO_2 -graphene composite, demonstrat-
30 ing the enhanced electron extraction and transport for TiO_2 -GD

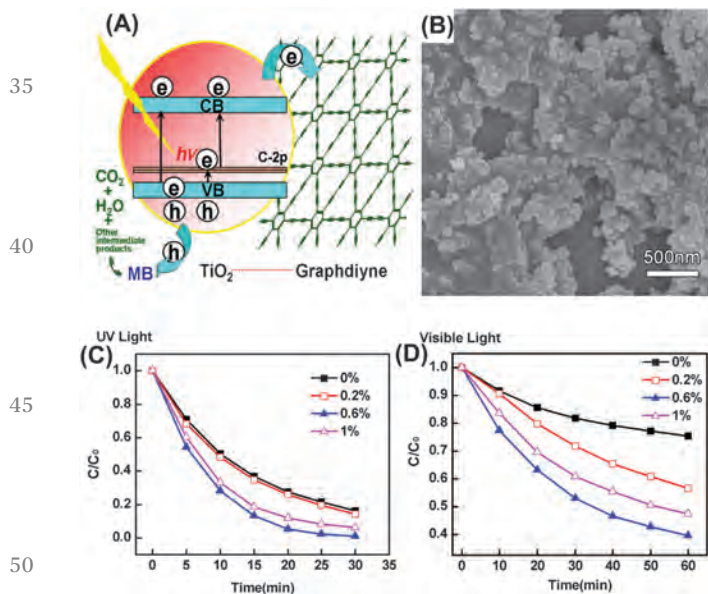


Fig. 19 (A) Schematic structure of P25-GD and proposed photodegradation
mechanism of methylene blue. (B) SEM image of P25-GD composite; (C, D)
Photocatalytic degradation of methylene blue under (C) UV and (D)
visible light irradiation with (A) P25, (B) P25-CNTs, (C) P25-graphene, and
(D) P25-GD photocatalysts. Reproduced with permission of Wiley from
ref. 49. Copyright 2012.

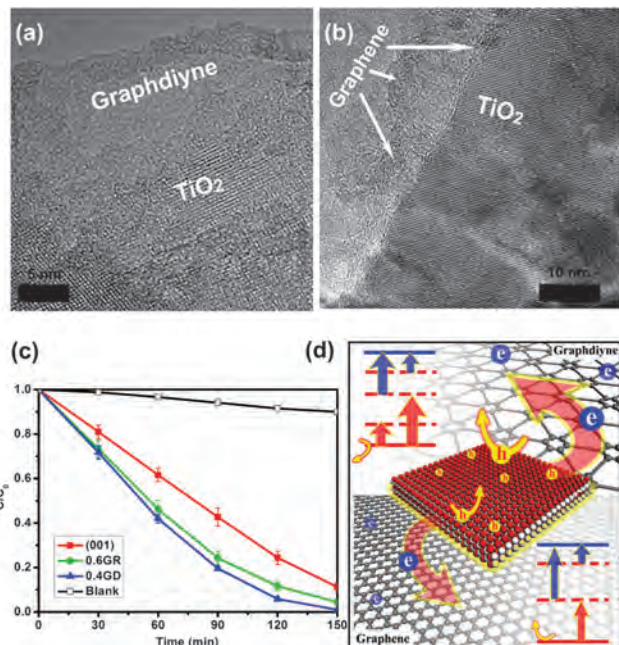


Fig. 20 HRTEM images of (a) TiO_2 -GD and (b) TiO_2 -graphene compo-
sites. (c) Photocatalytic degradation of methylene blue with TiO_2 , TiO_2 -
GD, TiO_2 -graphene composites, and the blank experiment (without any
photocatalyst). (d) The proposed photocatalytic degradation mechanism
of TiO_2 -GD and TiO_2 -graphene. Reproduced with permission of the
American Chemical Society from ref. 50. Copyright 2013.

composites. These results were confirmed by theoretical DFT
calculations that also showed TiO_2 -GD composites have a rich
electronic structure, rapid charge separation, and high oxida-
30 tive ability compared with pure TiO_2 or TiO_2 -graphene compo-
site, making them excellent photocatalysts. These results
suggest GD will become a superb competitor among the 2D
carbon materials available for photocatalytic applications.

6. Summary

This tutorial review provides a concise overview of synthesis
and functionalization of graphene, while also providing a snap
shot of its up-to-date achievements in photovoltaic and photo-
35 catalytic applications. Graphene is currently the material of
choice for enhancing the efficiency of photoconversion devices
due to its unique atom-thick 2D structure and excellent elec-
trical, thermal, mechanical, and optical properties. In addition,
its inherent flexibility and chemical robustness allow for pre-
40 viously unattainable device functionality, for example as a
replacement for rigid ITO electrodes that has enabled the
production of flexible solar cells. Graphyne and graphdiyne,
two new and hotly debated carbon allotropes, have been pre-
dicted to have mechanical and electrical properties as similar
45 as, if not much better than graphene. More impressively, unlike
graphene, they demonstrate an intrinsic semiconducting na-
ture and various types of substructures, implying great poten-
tial in photoconversion. As 2D carbon allotropes, all three materials

1 showed great benefits in numerous aspects of photoconversion technologies.

To summarize, 2D carbon allotropes enhance the efficiency of photoelectric conversion and photocatalytic activity in three primary ways. Firstly, all three carbon materials have high specific surface area that physically bridges the gaps between semiconductor nanoparticles or bulk heterojunctions to maintain electrical contact and lower interfacial resistance. They can bend, twist, and wrap around nanomaterials to form an interpenetrating percolated electron transport conduit, far surpassing the charge transport enhancement capabilities of 1D materials such as CNTs. For graphene, the strong van der Waal forces between 2D carbon layers provide good adhesion to surfaces and ensure multiple points of electrical contact, while its high basal surface area provides numerous additional active sites for photocatalytic conversion reactions.

Secondly, 2D carbon allotropes enhance charge separation in photoabsorbing semiconductors, dyes, and conjugated polymers. Excitonic recombination is a burgeoning challenge for photoconversion devices and can dramatically limit efficiency. Once formed, excitons have a finite pico- to micro-second excited state lifetime and must be efficiently separated and extracted before recombination—if not, the photons are wasted. When composited with TiO₂ nanoparticles, they have shown to effectively separate electrons from holes, and even store delocalized electrons for an extended period of time. They efficiently extract charge from photoabsorbing materials in OPVs, DSSCs, and photocatalysts, and also inhibit recombination to maximize light collection and photoconversion.

Lastly, the introduction of 2D carbon allotropes to photoconversion devices increases efficiency by rapidly extracting photogenerated charges to active surfaces or through external circuits. Their superb charge transport properties have made them the choice material for enhancing electron conductivity and mobility through almost every layer, electrode, and interface in photoconversion devices. They are on their way to revolutionizing photovoltaic and display technologies by becoming a cost-effective and mechanically flexible alternative to ITO transparent conducting electrodes.

Notably, for graphyne and graphdiyne, though less experimental studies have been reported due largely to the unavailability of free-standing graphynes in the laboratory, according to theoretical calculations they are predicted to possess exceptional electronic and optical properties compared with graphene, suggesting a potential direction for fabrication of novel nanoelectronic and optoelectronic devices. Also large area graphdiyne films have been synthesized and when used as additives to optoelectronic devices and photocatalysis, they show greatly enhanced performance, which may be due to their 2D nature like graphene accompanying the high specific surface area and superb charge transport capability.

7. Perspective

Graphene is the latest carbon material to win the interests of the scientific community, and its initial successes in photoelectric conversion and catalysis are the first step on its revolutionary path. Despite many examples demonstrating its outstanding efficacy for photoconversion technologies, the field is still in its preliminary stages, and significant challenges remain—particularly in producing large area/volume defect-free graphene with controlled surface chemistry. Scalable methods for producing chemically versatile graphene with exceptional electrical properties will undoubtedly lead to the commercialization of a number of verging photoconversion technologies. Overcoming these challenges will require innovations in the synthesis, chemical functionalization, and our improved theoretical understanding of charge separation and transport in specific device architectures.

Producing large area/volume defect-free graphene with controlled surface chemistry will be essential for the eventual commercialization of graphene. However, there currently exists a compromise between structure and function, and the dominant methods to produce graphene—vapour phase CVD and solution-based oxidation–exfoliation–reduction of graphite—are diverging in their attempts to resolve the same challenges. CVD methods are largely focused on replacing transparent ITO electrodes, but there are still challenges with reducing the sheet resistance, increasing carrier mobility, and uniformly doped large area films. For most photovoltaic and photocatalytic applications where graphene is composited with semiconductors or conjugated polymers, solution-derived graphene is the only option. However, with solution processability comes numerous defects, undefined surface chemistries, and very high resistance. Perhaps high throughput strategies to growing graphene films directly on the surface (or a sacrificial metallic surface) of semiconductor nanoparticles in solution or supercritical solvents would provide direct routes to composite materials with high quality graphene. Regardless, designing a hybrid CVD/solution-based method would help solve a variety of synthetic challenges facing researchers today.

Detailed theoretical and mechanistic studies will also help to fully understand how the electronic interactions between graphene and semiconductor materials enhance charge separation and transport to enhance solar cell efficiency and photocatalysis activity. This would lead to rationally designed graphene-based composites with optimized interfacial engineering that makes full use of its unique structural and electronic properties to achieve superior photoconversion performance. Studying alternative 2D analogues of graphene such as graphyne or graphdiyne, in addition to alternative 2D materials such as h-BN and metal chalcogenide films, will further identify the intrinsic aspects of graphene that make it such a promising material for photoconversion applications.

Graphyne and graphdiyne are emerging materials that have theoretically shown to have as much, if not more potential than graphene in photoconversion and optoelectronic technologies. The proposed high charge carriers mobility and intrinsic

1 semiconducting properties, will surely guarantee them to play
their roles in a variety of electronic and optoelectronic devices.
Also in some other areas which also need the fascinating charge
mobility, such as lithium ion battery and fuel cells, graphyne
5 and graphdiyne will also have their places and a lot of efforts
are needed to be done. For the bandgap, graphyne and graph-
diyne can be semiconductors or metal depending on its stack-
ing configuration. The methods of chemical functionalization
and doping can be also transferred to graphyne and graphdiyne
10 and their band structures can be entailed and modified. Also
with the various types of graphynes family due to the different
percentage of acetylenic linkages, some novel mechanical and
electronic structures are anticipated to be obtained. For exam-
ple, the specific example of 6,6,12-graphyne, which has a
15 rectangular lattice arrangement, indicates that this material
in some aspects is more versatile than graphene, due to its
directional anisotropy and its non-equivalent Dirac points.
However, though a few synthetic studies of graphdiyne films
and nanoribbons have been reported, the large quantities of
20 graphyne and graphdiyne with high quality and purity are still
unseen. Significant effort should be dedicated to designing and
producing tangible amounts of high-purity graphyne and
graphdiyne to verify recent theoretical predictions, and until
effective methods are found, graphene will continue to reign
25 supreme as the penultimate 2D carbon allotrope.

Finally, although considerable progress has been achieved,
the studies of 2D carbon allotropes in photoelectric conversion
and catalysis are still in their preliminary stages. Learning from
silicon, which dominated the semiconductor industry due to its
30 intrinsic properties, abundance and the ease with which it can
be processed, it is hard to fully exploit the strongest or most
valuable use for a novel material in so short a period. Keep
patient and guarded optimism. Things are, after all, off to a
good start.

35

Acknowledgements

We are grateful for financial support from the National Natural
40 Science Foundation of China (No. 21031005, 21203201,
51072020, 21271021, 51202248, 21203201, 51172235,
51272165), National Science Fund for Distinguished Young
Scholars (No. 21325105), the Foundation for State Key Labora-
tory of Multiphase Complex Systems (No. MPCs-2012-A-08).

45

References

- 1 A. K. Geim and K. S. Novoselov, *Nat. Mater.*, 2007, **6**, 183.
2 Y. Zhu, D. K. James and J. M. Tour, *Adv. Mater.*, 2012,
50 **24**, 4924.
3 V. Georgakilas, M. Otyepka, A. B. Bourlinos, V. Chandra,
N. Kim, K. C. Kemp, P. Hobza, R. Zboril and K. S. Kim,
Chem. Rev., 2012, **112**, 6156.
4 X. Huang, X. Qi, F. Boey and H. Zhang, *Chem. Soc. Rev.*,
55 **2012**, **41**, 666.

- 5 J. Chen, J. Xi, D. Wang and Z. Shuai, *J. Phys. Chem. Lett.*,
2013, **4**, 1443.
6 K. S. Novoselov, A. K. Geim, S. V. Morozov, D. Jiang,
Y. Zhang, S. V. Dubonos, I. V. Grigorieva and A. A. Firsov,
Science, 2004, **306**, 666. 5
7 Z. Yan, J. Lin, Z. Peng, Z. Sun, Y. Zhu, L. Li, C. Xiang,
E. L. Samuel, C. Kittrell and J. M. Tour, *ACS Nano*, 2012,
6, 9110.
8 K. V. Emtsev, A. Bostwick, K. Horn, J. Jobst, G. L. Kellogg,
L. Ley, J. L. McChesney, T. Ohta, S. A. Reshanov, J. Röhr,
10 E. Rotenberg, A. K. Schemid, D. Waldmann, H. B. Weber
and T. Seyller, *Nat. Mater.*, 2009, **8**, 203.
9 H. Bai, C. Li and G. Shi, *Adv. Mater.*, 2011, **23**, 1089.
10 Y. Hernandez, V. Nicolosi, M. Lotyo, F. M. Blighe, Z. Sun,
S. De, I. T. Mcgovern, B. Holland, M. Byrne, Y. K. Gun'ko,
15 J. J. Boland, P. Niraj, G. Duesberg, S. Krishnamurthy,
R. Goodhue, J. Hutchison, V. Scardaci, A. C. Ferrari and
J. N. Coleman, *Nat. Nanotechnol.*, 2008, **3**, 563.
11 B. Genorio, W. Lu, A. M. Dimiev, Y. Zhu, A.-R. O. Raji,
B. Novosel, L. B. Alemany and J. M. Tour, *ACS Nano*, 2012,
20 **6**, 4231.
12 X. Feng, M. Liu, W. Pisula, M. Takase, J. Li and K. Müllen,
Adv. Mater., 2008, **20**, 2684.
13 E. Bekyarova, M. E. Itkis, P. Ramesh, C. Berger, M. Sprinkle,
W. A. de Heer and R. C. Haddon, *J. Am. Chem. Soc.*, 2009,
25 **131**, 1336.
14 X. Wang, X. Li, L. Zhang, Y. Yoon, P. K. Weber, H. Wang,
J. Guo and H. Dai, *Science*, 2009, **324**, 768.
15 G. Eda, G. Ganchini and M. Chhowalla, *Nat. Nanotechnol.*,
2010, **3**, 270. 30
16 T.-K. Hong, D. W. Lee, H. J. Choi, H. S. Shin and B.-S. Kim,
ACS Nano, 2010, **4**, 3861.
17 S. Bae, H. Kim, Y. Lee, X. Xu, J.-S. Park, Y. Zheng,
J. Balakrishnan, T. Lei, H. R. Kim, Y. I. Song, Y.-J. Kim,
K. S. Kim, B. Ozyilmaz, J.-H. Ahn, B. H. Hong and S. Lijima,
35 *Nat. Nanotechnol.*, 2010, **5**, 574.
18 Z. Yin, S. Sun, T. Salim, S. Wu, X. Huang, Q. He, Y. M. Lam
and H. Zhang, *ACS Nano*, 2010, **4**, 5263.
19 X. Wang, L. Zhi and K. Müllen, *Nano Lett.*, 2008, **8**, 327.
20 T. W. Hamann, R. A. Jensen, A. B. F. Martins, H. V. Ryswyk
and J. T. Hupp, *Energy Environ. Sci.*, 2008, **1**, 66. 40
21 N. Yang, J. Zhai, D. Wang, Y. Chen and L. Jiang, *ACS Nano*,
2010, **4**, 887.
22 N. Yang, Y. Zhang, J. E. Halpert, J. Zhai, D. Wang and
L. Jiang, *Small*, 2012, **8**, 1762. 45
23 J. D. Roy-Mayhew, D. J. Bozym, C. Punckt and I. A. Aksay,
ACS Nano, 2010, **4**, 6203.
24 X. Yan, X. Cui, B. Li and L.-S. Li, *Nano Lett.*, 2010, **10**, 1869.
25 G. Li, R. Zhu and Y. Yang, *Nat. Photonics*, 2012, **6**, 153.
26 Z. Liu, Q. Liu, Y. Huang, Y. Ma, S. Yin, X. Zhang, W. Sun and
Y. Chen, *Adv. Mater.*, 2008, **20**, 3924. 50
27 S.-S. Li, K.-H. Tu, C.-C. Lin, C.-W. Chen and M. Chhowalla,
ACS Nano, 2010, **4**, 3169.
28 C. X. Guo, H. B. Yang, Z. M. Sheng, Z. S. Lu, Q. L. Song and
C. M. Li, *Angew. Chem., Int. Ed.*, 2010, **49**, 3014. 55

- 1 29 Y. Li, Y. Hu, Y. Zhao, G. Shi, L. Deng, Y. Hou and L. Qu, *Adv. Mater.*, 2011, **23**, 776.
- 30 Q. Xiang, J. Yu and M. Jaroniec, *Chem. Soc. Rev.*, 2012, **41**, 782.
- 5 31 I. V. Lightcap, T. H. Kosel and P. V. Kamat, *Nano Lett.*, 2010, **10**, 577.
- 32 H. Zhang, X. Lv, Y. Li, Y. Wang and J. Li, *ACS Nano*, 2010, **4**, 380.
- 33 J. Du, X. Lai, N. Yang, J. Zhai, D. Kisailus, F. Su, D. Wang and L. Jiang, *ACS Nano*, 2010, **5**, 590.
- 10 34 O. Akhavan and E. Ghaderi, *J. Phys. Chem. C*, 2009, **113**, 20214.
- 35 G. Xie, K. Zhang, B. Guo, Q. Liu, L. Fang and J. R. Gong, *Adv. Mater.*, 2013, **25**, 3820.
- 15 36 W. Fan, Q. Lai, Q. Zhang and Y. Wang, *J. Phys. Chem. C*, 2011, **115**, 10694.
- 37 Q. Xiang, J. Yu and M. Jaroniec, *J. Am. Chem. Soc.*, 2012, **134**, 6575.
- 38 Q. Li, B. Guo, J. Yu, J. Ran, B. Zhang, H. Yan and J. R. Gong, *J. Am. Chem. Soc.*, 2011, **133**, 10878.
- 20 39 Y. Hou, F. Zou, A. Dagg and P. Feng, *Nano Lett.*, 2012, **12**, 6464.
- 40 T.-F. Yeh, J.-M. Syu, C. Cheng, T.-H. Chang and H. Teng, *Adv. Funct. Mater.*, 2010, **20**, 2255.
- 41 Y. Zhang, Z.-R. Tang, X. Fu and Y.-J. Xu, *ACS Nano*, 2011, **4**, 7303.
- 42 R. Baughman, H. Eckhardt and M. Kertesz, *J. Chem. Phys.*, 1987, **87**, 6687.
- 43 D. Malko, C. Neiss, F. Viñes and A. Görling, *Phys. Rev. Lett.*, 2012, **108**, 086804.
- 44 N. Narita, S. Nagai, S. Suzuki and K. Nakao, *Phys. Rev. B: Condens. Matter Mater. Phys.*, 1998, **58**, 11009.
- 10 45 M. Haley, S. Brand and J. Pak, *Angew. Chem., Int. Ed.*, 1997, **36**, 836.
- 46 M. Q. Long, L. Tang, D. Wang, Y. L. Li and Z. G. Shuai, *ACS Nano*, 2011, **5**, 2593.
- 47 G. Li, Y. Li, H. Liu, Y. Guo and D. Zhu, *Chem. Commun.*, 2010, **46**, 3256.
- 48 H. Du, Z. Deng, Z. Lü, Y. Yin, L. Yu, H. Wu, Z. Chen, Y. Zou, Y. Wang, H. Liu and Y. Li, *Synth. Met.*, 2011, **161**, 2055.
- 49 S. Wang, L. Yi, J. Halpert, X. Lai, Y. Liu, H. Cao, R. Yu, D. Wang and Y. Li, *Small*, 2012, **8**, 265.
- 20 50 N. Yang, Y. Liu, H. Wen, Z. Tang, H. Zhao, Y. Li and D. Wang, *ACS Nano*, 2013, **7**, 1504.

25

25

30

30

35

35

40

40

45

45

50

50

55

55